Ph.D. DISSERTATION

STRATEGY FOR IMPROVING RELIABILITY OF POWER LINE COMMUNICATIONS WITH APPLICATIONS TO SMART GRID

스마트 그리드를 위한 전력선 통신의 신뢰성 향상 기법 연구

BY

YU-SUK SUNG

AUGUST 2014

DEPARTMENT OF ELECTRICAL ENGINEERING AND
COMPUTER SCIENCE
COLLEGE OF ENGINEERING
SEOUL NATIONAL UNIVERSITY

Ph.D. DISSERTATION

STRATEGY FOR IMPROVING RELIABILITY OF POWER LINE COMMUNICATIONS WITH APPLICATIONS TO SMART GRID

스마트 그리드를 위한 전력선 통신의 신뢰성 향상 기법 연구

BY

YU-SUK SUNG

AUGUST 2014

DEPARTMENT OF ELECTRICAL ENGINEERING AND
COMPUTER SCIENCE
COLLEGE OF ENGINEERING
SEOUL NATIONAL UNIVERSITY

STRATEGY FOR IMPROVING RELIABILITY OF POWER LINE COMMUNICATIONS WITH APPLICATIONS TO SMART GRID

지도교수 김 성 철

이 논문을 공학박사 학위논문으로 제출함
2014 년 4 월

서울대학교 대학원
전기·컴퓨터공학부
성 유 석

성유석의 박사학위논문을 인준함
2014 년 6 월

위 원 장 박 세 웅 (인) S Bahk
부위원장 김 성 철 (인) C. Kim
위 원 김 남 수 (인)
위 원 이 종 호 (인)
위 원 김 용 화 (인)

Abstract

STRATEGY FOR IMPROVING RELIABILITY OF POWER LINE COMMUNICATIONS WITH APPLICATIONS TO SMART GRID

YU-SUK SUNG

DEPARTMENT OF ELECTRICAL ENGINEERING AND COMPUTER SCIENCE

COLLEGE OF ENGINEERING

THE GRADUATE SCHOOL

SEOUL NATIONAL UNIVERSITY

To solve the problems of global warming effects, rising energy-hungry demands, and risks of peak loads, many efforts to build a Smart Grid system are underway. A smart grid requires advanced information, and communication technologies to support its intelligent features, and it depends on the reliable data transmission via a communication network. Among the candidates of communication technology for smart grid, we focus on a power line communications (PLC), especially a broadband PLC over a medium voltage (MV) powerline network. The reliability of the PLC network are prerequisite for an appropriate communication medium for smart grid.

This dissertation considers a strategy to make the PLC network more reliable and robust. We consider a maximal ratio combining (MRC) diversity scheme for

a power line orthogonal frequency division multiplexing (OFDM) system. An optimal subcarrier pairing scheme is proposed to maximize the MRC gain. Numerical results are presented to verify that the proposed scheme provides enhanced performance.

Diversity gain comes at the expense of spectral loss. We adopt the precoding scheme proposed for wireless MIMO system to compensate the spectral loss due to the inherent transmission mechanism of the above subcarrier pairing scheme. It is shown that the proposed pairing scheme with higher modulation order achieves a comparable performance to the precoding scheme which requires high computational cost.

We extend the optimal subcarrier pairing with MRC approach to powerline/wireless diversity system, where the powerline and wireless subcarriers are paired to perform maximal ratio combining (MRC). An similar optimal subcarrier pairing scheme is proposed to maximize the data rate for MRC reception in powerline/wireless diversity OFDM systems. Numerical results show that, by using the proposed optimal subcarrier pairing, significant performance enhancement can be achieved in terms of Ergodic data rate and outage probability.

Keywords: Smart Grid, Power line communications, Reliability, Diversity, Maximal ratio combining, Subcarrier pairing

***Student Number*:** 2004–21537

Contents

List of Tables

List of Figures

Chapter 1

Introduction

1.1 Smart Grid

The power grids were designed decades ago, with the main aim of delivering electricity from large power stations to households and businesses [1]. To minimize the impact of climate change while at the same time maintaining social prosperity, smart energy must be embraced to ensure a balanced economical growth and environmental sustainability [2]. Therefore, in the last few years, the new concept of a '*Smart Grid*' became a critical enabler in the contemporary world and has attracted increasing attention of policy makers and engineers. A smart grid is an electricity network that uses digital and other advanced technologies to monitor and manage the transport of electricity from all generation sources to meet the varying electricity demands of end-users [3]. Smart grids coordinate the needs and capabilities of all generators, grid operators, end-users and electricity market stakeholders to operate all parts of the system as efficiently as possible, minimizing costs and environmental impacts while maximizing system reliability, resilience and stability. Technologies such as distributed generation and plug-in hybrid electric vehicles (PHEVs) will help to reduce CO_2 emissions and offer more sustainable options to consumers of energy, while applications such

as the advanced metering infrastructure (AMI) and home energy management system (HEMS) will enable consumers to manage their energy usage more efficiently [1].

Table 1.1: Comparison between the existing grid and the smart grid

Existing grid	Smart grid
Electromechanical	Digital
One-way communication	Two-way communication
Centralized generation	Distributed generation
Hierarchical	Network
Few sensors	Sensors throughout
Blind	Self-monitoring
Manual restoration	Self-healing
Failures and blackouts	Adaptive and islanding
Manual check/test	Remote check/test
Limited control	Pervasive control
Few customer choices	Many customer choices

Figure 1.1 shows the traditional electric grid. The electricity is first generated and then transmitted over long distances to the substations, then where it is further distributed to the consumers. A vision of the smart grid is illustrated in Figure 1.2. One significant difference between the traditional grid and the smart rid is two-way exchange of information between the consumer and the grid. A Smart Grid incorporates the benefits of advanced communications and information technologies to deliver real-time information and enable the near-instantaneous balance of supply and demand on the electrical grid. Table 1.1 gives a brief comparison between the existing grid and the smart grid [4]. The anticipated benefits and requirements of smart grid are the following [5, 6]:

- Improving power reliability and quality

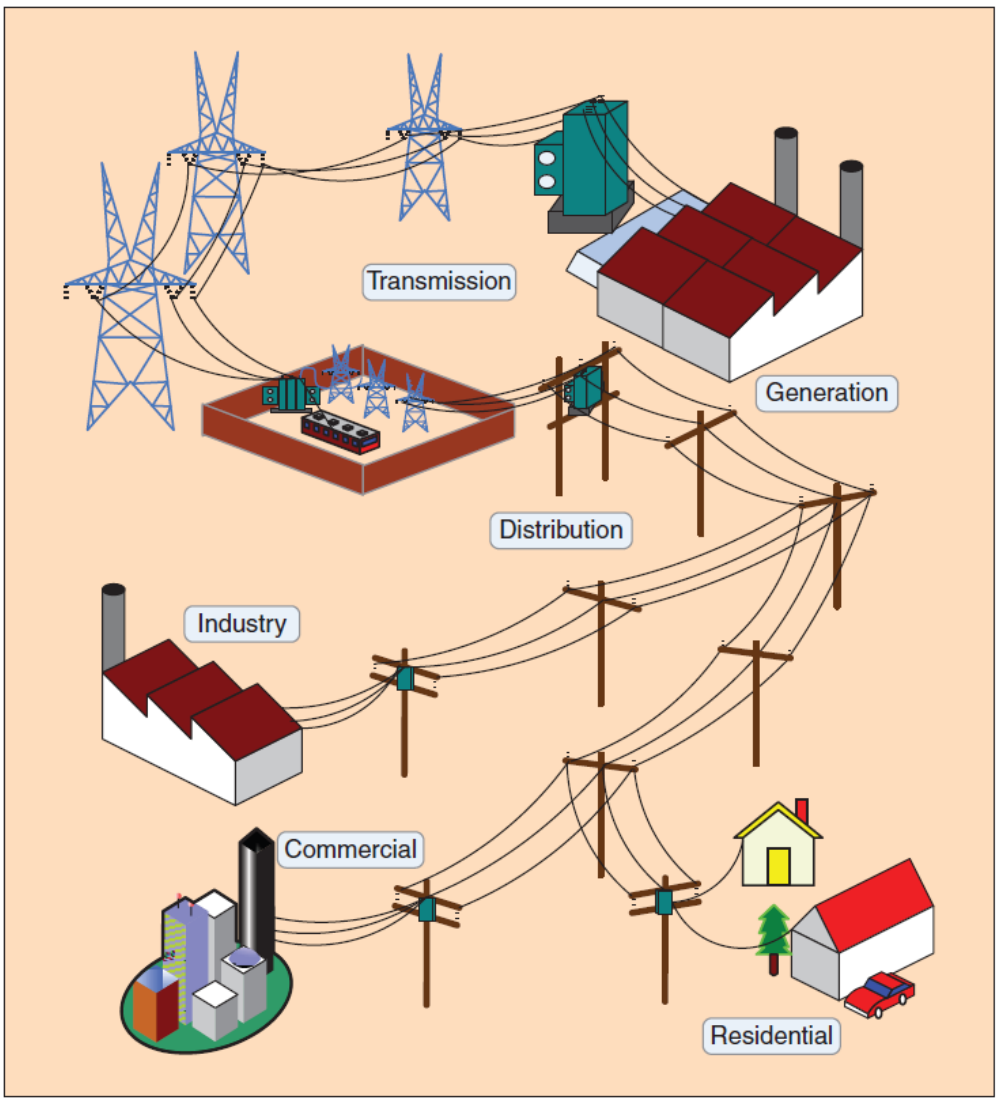

Figure 1.1: Traditional electric grid.

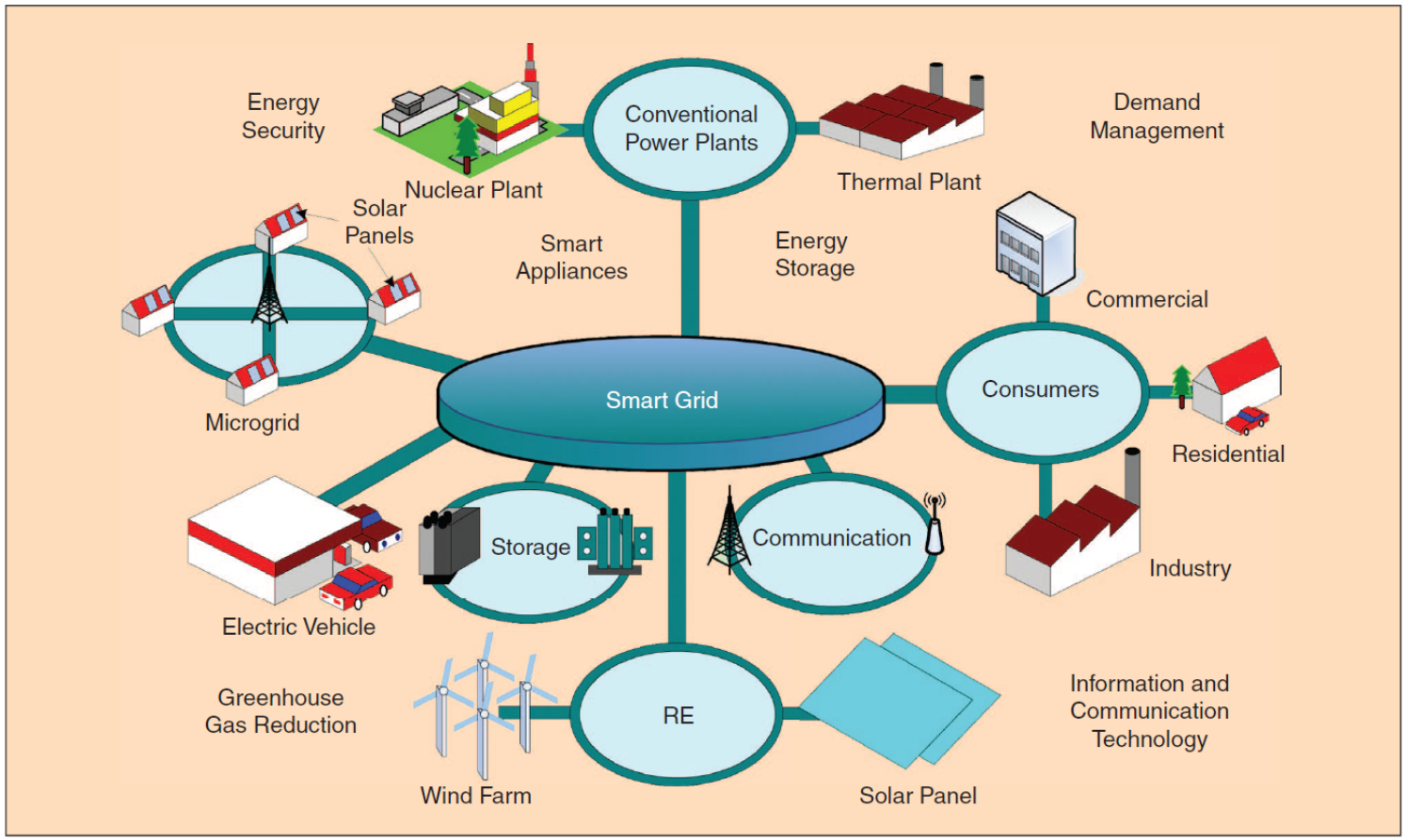

Figure 1.2: Smart grid.

- Optimizing facility utilization and averting construction of back-up (peak load) power plants
- Enhancing capacity and efficiency of existing electric power networks
- Improving resilience to disruption
- Enabling predictive maintenance and self-healing responses to system disturbances
- Facilitating expanded deployment of renewable energy sources
- Accommodating distributed power sources
- Automating maintenance and operation
- Reducing greenhouse gas emissions by enabling electric vehicles and new power sources
- Reducing oil consumption by reducing the need for inefficient generation during peak usage periods
- Presenting opportunities to improve grid security
- Enabling transition to plug-in electric vehicles and new energy storage options
- Increasing consumer choice
- Enabling new products, services, and markets.

1.2 Communication and Networking in the Smart Grid

In the smart grid, reliable and real-time information becomes the key factor for reliable delivery of power from the generating units to the end-users [7]. With the integration

of advanced technologies and applications for achieving a smarter electricity grid infrastructure, a huge amount of data from different applications will be generated for further analysis, control and real-time pricing methods. Hence, it is very critical for to define the communications requirements and find the best communications infrastructure to handle the output data and deliver a reliable, secure and cost-effective service throughout the total system.

1.2.1 Network Topologies

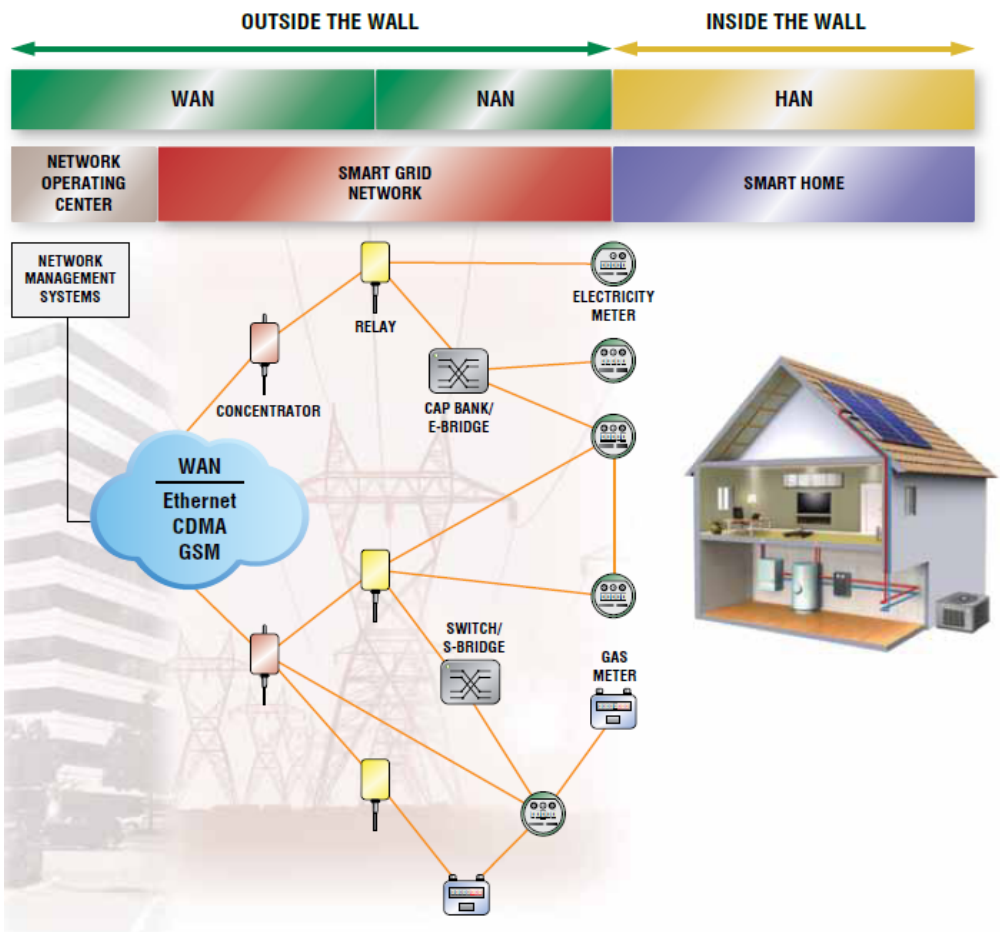

Figure 1.3: Network topologies of Smart Grid.

From a networking topological viewpoint, smart grid communication entities can be divided into three types of network architecture, namely the Home Area Network (HAN), the Neighboring Area Network (NAN) and the Wide Area Network (WAN) (Figure 1.3). In the following, a brief description of the transmission categories is given [8].

Wide Area Network (WAN)

WAN provides communication between the electric utility and substations. WAN should span all over the substations, distributed power generation and storage facilities, distribution assets, such as capacitor banks, transformers, and reclosers to be fully effective and scalable enough. It is a high-bandwidth backbone communication network that handles long-distance data transmission with advance monitoring and sensing applications. WAN provides a two-way communication network for communication, automation, and monitoring purposes of smart grid applications. Each smart grid application running on WAN has unique communication and Quality-of-Service (QoS) requirements. Some applications like wide-area situational awareness systems require real-time or near real-time responses; some of them, like substation automation, will require high bandwidth and fast response times; some applications, like AMI, will need considerable bandwidth and broadband data rates.

Neighboring Area Network (NAN)

NAN can be described as the communication network for power distribution areas and includes distribution automation and control devices communicating over networks between individual service connections and backhaul points to the electric utilities. NAN acts as a bridge between customer premises and substations with collectors, access points and data concentrators. Intelligent nodes are deployed between customer premises and substations to collect and control the data from surrounding data points.

These nodes are connected to a centralized gateway, which is always supported by electric utilities to transmit the collected data. Low bandwidth NAN channels are highly robust for reliable data communication. A NAN is ubiquitous and broadband wireless resource that meets the utility requirements for reliability and resilience. The coverage area includes urban-suburban and rural environments. A NAN is highly supported by advanced metering infrastructure deployments and it is rapidly expanding the range of its application areas, e.g., advanced distribution automation and integration of distributed energy resources.

Home Area Network (HAN)

Smart meters will have the ability to connect to the HAN, and this will enable consumers to be aware of electricity usage costs and manage their consumption behaviors and take control of smart appliances. Home area networks support low-bandwidth communication between home electrical appliances and smart meters. The primary task of in-home applications is to inform customers about the consumption behaviors via home displays or a web interface. Hence, the bandwidth needs are between 10 and 100 kbps per device and there is no urgent need for low latency. However, it is expected that new functions will quickly be integrated, thus implementing intelligent load management. Low-bandwidth, slow-speed, cost-effective, and flexible connections are preferred for HAN.

1.2.2 Communication Technologies for the Smart Grid

A variety of diverse communication technologies are available to perform different tasks within the smart grid, ranging from usage data collection and transmission, through to monitoring generation and distribution. Some of the most promising technologies will now be reviewed.

ZigBee

ZigBee is considered as a good option for metering and energy management and ideal for smart grid implementations along with its simplicity, mobility, robustness, low bandwidth requirements, low cost of deployment, its operation within an unlicensed spectrum, easy network implementation, being a standardized protocol based on the IEEE 802.15.4 standard. However, there are some constraints on ZigBee for practical implementations, such as low processing capabilities, small memory size, small delay requirements and being subject to interference with other appliances, which share the same transmission medium, license-free industrial, scientific and medical (ISM) frequency band ranging from IEEE 802.11 wireless local area networks (WLANs), WiFi, Bluetooth and Microwave.

Wireless Mesh

Wireless mesh networking is a cost effective solution with dynamic self-organization, self-healing, self-configuration, high scalability services, which provide many advantages, such as improving the network performance, balancing the load on the network, extending the network coverage range. Advanced metering infrastructures and home energy management are some of the applications that wireless mesh technology can be used for. Network capacity, fading and interference can be counted as the major challenges of wireless mesh networking systems. Providing the balance between reliable and flexible routing, a sufficient number of smart nodes, taking into account node cost, are very critical for mesh networks.

Cellular Network Communication

Existing cellular networks can be a good option for communicating between smart meters and the utility and between far nodes. The existing communications infrastructure avoids utilities from spending operational costs and additional time for building a ded-

icated communications infrastructure. Cellular network solutions also enable smart metering deployments spreading to a wide area environment. 2G, 2.5G, 3G, WiMAX, and LTE are the cellular communication technologies available to utilities for smart metering deployments. However, the services of cellular networks are shared by customer market and this may result in network congestion or decrease in network performance in emergency situations. Hence, these considerations can drive utilities to build their own private communications network. In abnormal situations, such as a wind storm, cellular network providers may not provide guarantee service.

Digital Subscriber Line (DSL)

Digital Subscriber Lines (DSLs) is a high-speed digital data transmission technology that uses the wires of the voice telephone network. The widespread availability, low-cost and high bandwidth data transmissions are the most important reasons for making the DSL technology the first communications candidate for electricity suppliers in implementing the smart grid concept with smart metering and data transmission smart grid applications. However, the reliability and potential down time of DSL technology may not be acceptable for mission critical applications. The wired DSL-based communications systems require communications cables to be installed and regularly maintained, and thus, cannot be implemented in rural areas due to the high cost of installing fixed infrastructure for low-density areas.

Power Line Communication (PLC)

PLC can be considered as a promising technology for smart grid applications due to the fact that the existing infrastructure decreases the installation cost of the communications infrastructure. The standardization efforts on PLC networks, the cost-effective, ubiquitous nature, and widely available infrastructure of PLC, can be the reasons for its strength and popularity. HAN application is one of the biggest applications for PLC

technology. Moreover, PLC technology can be well suited to urban areas for smart grid applications, such as smart metering, monitoring and control applications, since the PLC infrastructure is already covering the areas that are in the range of the service territory of utility companies. However, there are some technical challenges due to the nature of the powerline networks. The powerline transmission medium is a harsh and noisy environment that makes the channel difficult to be modeled. Furthermore, the network topology, the number and type of the devices connected to the powerlines, wiring distance between transmitter and receiver, all, adversely affect the quality of signal, that is transmitted over the powerlines

1.3 Dissertation Outline

The rest of the dissertation is organized as follows. In Chapter 2, more detailed PLC characteristics are reviewed and implementation of PLC channel and noise which are used for simulation in remaining chapters are described. In Chapter 3, an optimal subcarrier pairing with MRC diversity scheme is proposed for PLC OFDM system and numerical results are presented. A method to compensate the spectral loss due to the diversity transmission of proposed pairing scheme is also discussed. Optimal subcarrier pairing scheme is extended to the powerline/wireless diversity system in Chapter 4. Performance enhancements are evaluated in terms of Ergodic data rate and outage probability. Finally, we draw conclusions and address future research directions in Chapter 5.

Chapter 2

Power Line Communications for Smart Grid

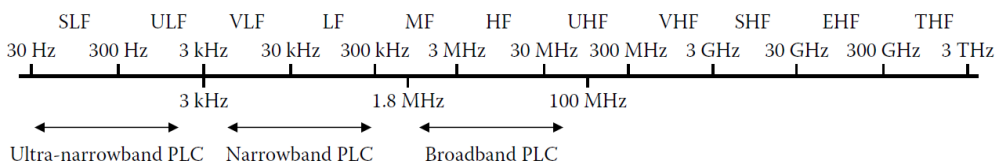

Figure 2.1: ITU frequency bands and their usage in power line communications.

One of the earliest initiatives for the automation of the electricity grid was taken using the power line communication (PLC) technology. The PLC technology involves introduction of a modulated carrier signal over the existing power line cable infrastructure for two way communication. As indicated in Figure 2.1, currently only the VLF up to the UHF bands are interesting for PLC systems. These systems are usually subdivided into narrowband (NB) and broadband (BB) PLC; the former operating below 1.8 MHz, the latter operating above. Detailed categorization and related standards are as follows [9]:

- Narrowband (NB): Technologies operating in the VLF/LF/MF bands (3–500 kHz), which include the European CENELEC (Comite Europeen de Normalisation Electrotechnique) bands (3–148.5 kHz), the US FCC (Federal Communications

Commission) band (9–490 kHz), the Japanese ARIB (Association of Radio Industries and Businesses) band (10–450 kHz), and the Chinese band (3–500 kHz). We can identify two sub-categories in NB-PLC:

  - Low Data Rate (LDR): Single carrier technologies capable of data rates of few kbit/s. Typical examples of LDR NB-PLC technologies are devices conforming to the following recommendations: ISO/IEC 14908-3 (LonWorks), ISO/IEC 14543-3-5 (KNX), CEA-600.31 (CEBus), IEC 61334-5-2, and IEC 61334-5-1 (FSK and Spread-FSK). Non-SDO based examples are Insteon, X10, HomePlug C&C, SITRED, Ariane Controls, and BacNet.

  - High Data Rate (HDR): Multicarrier technologies capable of data rates ranging between tens of kbit/s and up to 500 kbit/s. Typical examples of existing HDR NB-PLC technologies are ITU-T Recommendations G.9902 (G.hnem), G.9903 (G3-PLC), and G.9904 (PRIME). Additional non- SDO examples are PRIME and G3-PLC, which started as open specifications developed in industry alliances, but now have been approved as ITU-T standards.

- Broadband (BB): Technologies operating in the HF/VHF bands (1.8–250 MHz) and having a PHY rate ranging from several Mbps to several hundred Mbps. Typical examples of BB-PLC technologies are devices conforming to the TIA-1113 (HomePlug 1.0), IEEE 1901, ITU-T G.hn (G.9960/G.9961) recommendations. Non-SDO based examples are HomePlug AV 2.0, HomePlug Green PHY, UPA Powermax, and Gigle MediaXtreme.

Besides the distinction into NB-PLC and BB-PLC, it has been common practice to distinguish power line topologies according to operation voltages of the power lines [10].

- High-voltage (HV) lines, with voltages in the range from 110 to 380 kV, are used for nationwide or even international power transfer and consist of long

overhead lines with little or no branches. This makes them acceptable wave guides with less attenuation per line length as for their medium-voltage (MV) and low-voltage (LV) counterparts. However, their potential for BB communication services has up to the present day been limited. Time-varying HV arcing and corona noise with noise power fluctuations in the order of several tens of dBs as well as the practicalities and costs of coupling communication signals in and out of these lines have been an issue.

- MV lines, with voltages in the range from 10 to 30 kV, are connected to the HV lines via primary transformer substations. The MV lines are used for power distribution between cities, towns and larger industrial customers. They can be realized as overhead or underground lines. Further, they exhibit a low level of branches and directly connect to intelligent electronic devices (IED) such as reclosers, sectionalizers, capacitor banks and phasor measurement units. IED monitoring and control requires only relatively low data rates and NB-PLC can provide economically competitive communication solutions for these tasks.

- LV lines, with voltages in the range from 110 to 400 V, are connected to the MV lines via secondary transformer substations. A communication signal on an MV line can pass through the secondary transformer onto the LV line, however, with a heavy attenuation in the order of 55–75 dB. Hence, a special coupling device (inductive, capacitive) or a PLC repeater is frequently required if one wants to establish a high data rate communications path. The LV lines lead directly or over street cabinets to the end customers premises. Considerable regional topology difference exits.

2.1 Power Line Channel Characteristics

The power line channel and noise situations heavily depend on the scenario. But, in general, frequency-selective multi-path fading, a low-pass behavior, AC-related cyclic short-term variations and abrupt long-term variations can be observed.

Multi-path fading is caused by inhomogeneities of the power line segments where cabling and connected loads with different impedances give rise to signal reflections and in the sequel in-phase and anti-phase combinations of the arriving signal components. Besides multi-path fading, the PLC channel exhibits time variation due to loads and/or line segments being connected or disconnected.

2.2 PLC Channel Modeling [11]

Two kinds of PLC channel modeling approaches can be found in literature, namely the top-down approach and the bottom-up approach. A top-down approach attempts to find the most fitted model from measurements (either impulse responses or frequency responses) by means of data fitting, while in a bottom-up approach the channel model is derived from transmission line theory without relying on any measurement.

Top-Down Approach

Similar to wireless channel modeling, this approach treats the PLC channel as a black box and a large number of measurements are collected by exciting the channel with a reference signal in either time domain or frequency domain. Complex fitting algorithms are then applied in order to find a model that fits the measurements well. The fitting process includes identification of proper parameters and estimation of those parameters. The objective is to use a few parameters to approximate the channel with high accuracy.

This approach is advantageous in that the developed models are usually easy to use

and they allow fast channel generation. This makes them suitable for running Monte Carlo simulation, where a large number of channel realizations are required. With the help of the statistical results derived from measurements, the channel and even system performance may be studied analytically. The most significant disadvantage of this approach is its low flexibility. The model and its parameters derived for a specific network and frequency band may not be applied to other networks and frequency bands. Therefore, in order to develop a generalized top-down model, extensive channel measurements must be done globally. Another disadvantage is that it lacks physical connection with reality. For example, it is hard to use this model to describe the spatial correlation presented in power networks. Since power network is a bus system, it is possible that the received channel responses of two neighboring nodes have high correlation. Consequently, this approach may not be applied to network-related system modeling.

Bottom-Up approach

The bottom-up approach is usually based on transmission line theory. This approach requires perfect knowledge of the targeting power network, including its topology, the used power line cable and load impedances of terminals. These network elements are modeled mathematically so that they can be incorporated to generate the channel.

Transmission line theory was originally developed to describe electromagnetic (EM) wave propagation in a piece of transmission line with a bunch of partial differential equations (PDEs). Voltages along the transmission line were derived by solving these PDEs and incorporating reflections at line ends. The theory must be modified so that it can be applied to model signal propagation in a network. Voltage ratio approach, ABCD matrix and S-parameters are three popular methods in literature. Voltage ratio approach and ABCD matrix are basically the same method in different forms because they all focus on voltages and currents at network nodes. S-parameters approach is

different. It describes wave propagation in a network by utilizing transmission and reflection coefficients. Although this approach is complicated, it is directly related to signal propagation in a network. Therefore, it can be easily extended to the situation where different kinds of cables with different number of conductors are connected together. It is hard for a voltage ratio approach or an ABCD matrix approach to be applied to this situation.

The advantage of bottom-up approach is that it can be applied to various situations flexibly as long as the network information is perfectly known. In addition, this approach is closely related to the physics of power networks since it is derived from the physical interpretation of EM wave propagation in transmission line networks. Therefore, this approach can be used for network-related system modeling such as multiuser systems and relay systems. This approach also has several disadvantages. First, this approach is usually computational complex and the complexity grows with the complexity of the network. Second, this approach may not be practical since it only considers several key elements of a power network. A practical model should consider many other natural and artificial interference sources such as weather and radio. Finally, the collection of the aforementioned network elements (topology, cable, load) is challenge due to a large number of variations of them.

2.3 PLC Channel Noise Characteristics

The noise observed on indoor power line networks has been traditionally categorized into several classes, depending on its origin, its level and its time domain signature [12]. Power line noise can be grouped based on temporal as well as on spectral characteristics. As described in [13], one can distinguish colored background noise, narrowband (NB) noise, periodic impulsive noise asynchronous to the mains frequency, periodic impulsive noise synchronous to the mains frequency and aperiodic impulsive noise as indicated in Figure 2.2.

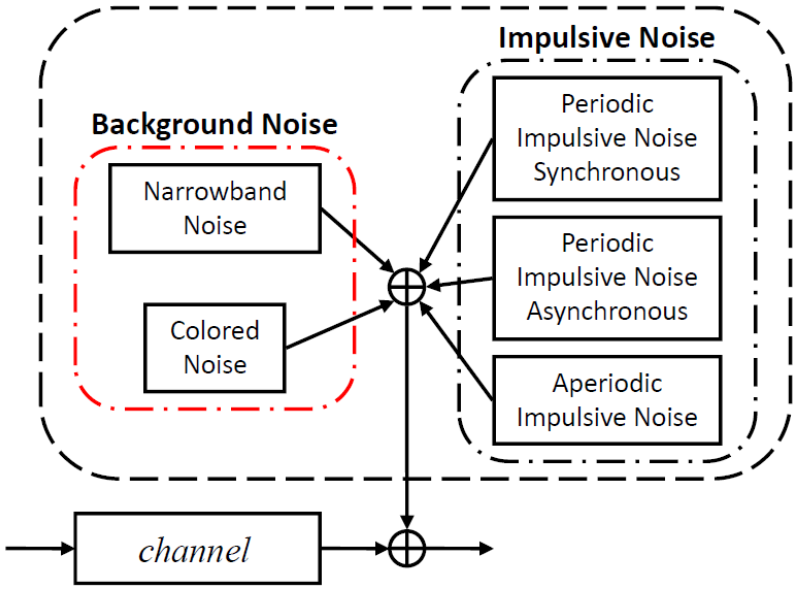

Figure 2.2: Classification of PLC noise.

A first class consists of the impulsive noise generated by electronic devices connected to the mains grid, such as switched mode power supplies, light dimmers or compact fluorescent lamps. This type of noise is of short duration (a few μs) but of relatively high level in the order of tens of mV. Due to the periodic nature of the mains, noisy devices can generate impulses in a synchronous way with the mains period. In this case, the impulsive noise is said to be periodic and synchronous to the mains frequency and presents a repetition rate at multiples of 50 or 60 Hz dependent on the mains frequency. Other noise sources generate impulses at a higher periodical rate up to several kHz, which are classified as periodic and asynchronous to the mains frequency. Finally, strong impulses can also be observed more sporadically, without any periodicity with the mains or with itself. This type of noise is sometimes referred to as aperiodic impulsive noise. The different characteristics of the impulsive noise have been statistically analyzed through the observation of experimental data in [14]. A comprehensive model of the PLC impulsive noise has been proposed in [12]. The

pulses are first statistically characterized in terms of amplitude, duration and repetition rate, and the global noise scenario is then modeled in the form of a Markov chain of noise states.

A second class of noise consists of narrowband (NB) noise. This type generally corresponds to ingress noise from broadcasting radio sources, in particular from the short-wave (SW) and frequency-modulation (FM) bands. Other ingress noise corresponds to leakages from nearby electrical or industrial equipment. This type of noise usually generates strong interference over long durations in a narrow frequency bandwidth in the order of tens of kHz.

Finally, the remaining noise sources, presenting a lower level of interference, form a third class of noise called background noise. The background noise is generally colored, in the sense that its power spectral density (PSD) is usually stronger at lower frequencies. In [15], the background noise PSD is modeled with decreasing power as a function of frequency.

2.4 MV Channel Description for This Dissertation

2.4.1 Implementation of Powerline Channel

The MV powerline channel model described in this dissertation adopts bottom-up approach, which is one of the deterministic approaches. This approach is preferred to simulate PLC networks with multiple nodes [16]. Among the established methods in bottom-up approach, the scattering matrix (SM) method [17, 18] is employed. The scattering matrix representation of a two-port network is convenient to evaluate its transfer function, so various topologies can be adapted.

For the SM method, the end-to-end MV network is separated into network modules, each of them comprise the successive branches. Referring to Figure 2.3 and Figure 2.4, the scattering matrix of a network module relates the incident wave $(a_1, a_2)^T$

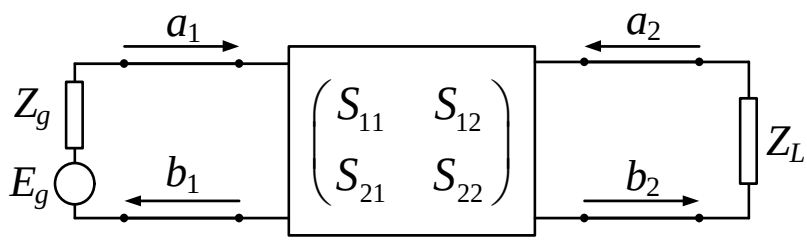

Figure 2.3: Two-port network model.

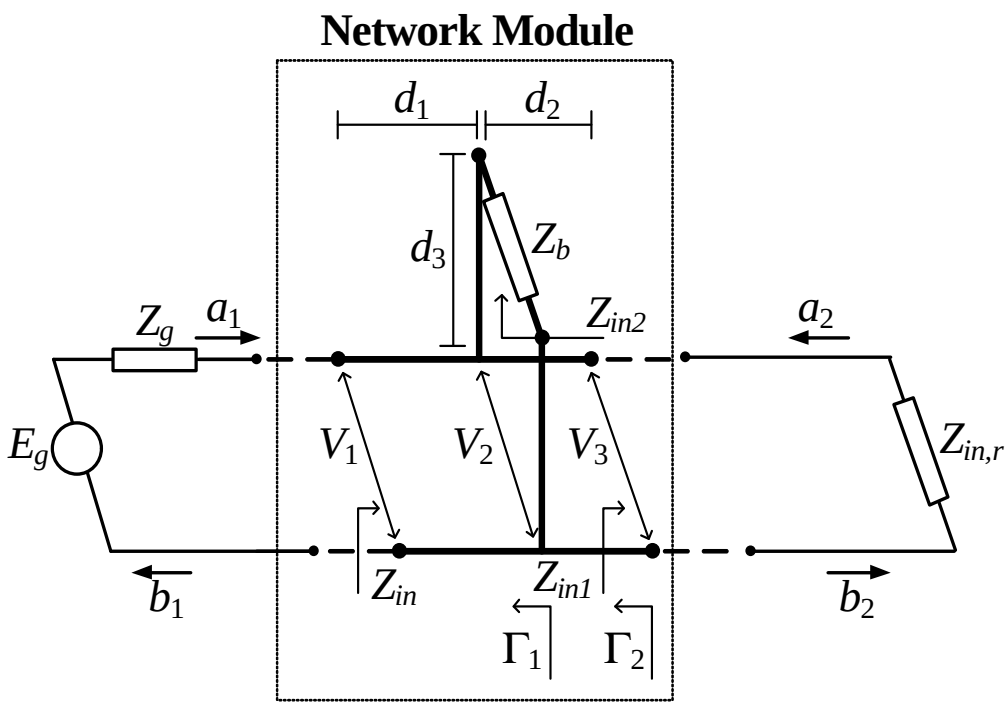

Figure 2.4: Connection of a network module.

and the reflected wave $(b_1, b_2)^T$ through

$$\begin{pmatrix} b_1 \\ b_2 \end{pmatrix} = \mathbf{S} \begin{pmatrix} a_1 \\ a_2 \end{pmatrix} = \begin{pmatrix} S_{11} & S_{12} \\ S_{21} & S_{22} \end{pmatrix} \begin{pmatrix} a_1 \\ a_2 \end{pmatrix} \tag{2.1}$$

In terms of the scattering matrix elements, the transfer function is given by S_{21}. The followings are the procedure to obtain end-to-end transfer function.

1) Evaluation of the scattering matrices of the network modules.

By using the transmission line theory, the elements of the scattering matrix S_{11}, S_{21} of a network module can be determined as

$$S_{11} = \frac{Z_{in} - Z_o}{Z_{in} + Z_o} \tag{2.2}$$

$$\begin{aligned} S_{21} &= 2\frac{V_3}{V_1} = 2\frac{V_3}{V_2}\frac{V_2}{V_1} \\ &= 2\frac{(1+\Gamma_1)e^{-\gamma d_1}}{1+\Gamma_1 e^{-\gamma d_1}} \frac{(1+\Gamma_2)e^{-\gamma d_2}}{1+\Gamma_2 e^{-\gamma d_2}} \end{aligned} \tag{2.3}$$

where Z_{in} is the input impedance, Z_o is the characteristic impedance, γ is the propagation constant, and Γ_1, Γ_2 are reflection coefficients. These modeling parameters are evaluated in [19]. For the first network module, S_{21} takes the value as follows:

$$S_{21} = 2\frac{V_3}{E_g} = 2\frac{(1+\Gamma_1)e^{-\gamma d_1}}{1+\Gamma_1 e^{-\gamma d_1}} \frac{(1+\Gamma_2)e^{-\gamma d_2}}{1+\Gamma_2 e^{-\gamma d_2}} \frac{Z_{in}}{Z_{in}+Z_g} \tag{2.4}$$

The elements S_{12} and S_{22} can be determined from (2.2), (2.3), and (2.4) by simply interchanging the source and the load.

2) Evaluation of the transmission matrices of the network modules.

The relationship between scattering matrix and transmission matrix is shown as follows:

$$\mathbf{T} = \begin{pmatrix} T_{11} & T_{12} \\ T_{21} & T_{22} \end{pmatrix} = \begin{pmatrix} \frac{1}{S_{21}} & -\frac{S_{22}}{S_{21}} \\ \frac{S_{11}}{S_{21}} & S_{12} - \frac{S_{11}S_{22}}{S_{21}}. \end{pmatrix} \tag{2.5}$$

3) Evaluation of the end-to-end transmission matrix.

Since the end-to-end MV power line network is the cascade of N network modules, the transmission matrix of the end-to-end MV power line network is given by

$$\mathbf{T} = \prod_{k=1}^{N} \mathbf{T_k} \tag{2.6}$$

where $\mathbf{T}_k$ is the transmission matrix for the k-th cascaded portion in the network.

4) Evaluation of the end-to-end transfer function.

The **S** matrix of the end-to-end MV power line network is obtained from

$$\mathbf{S} = \begin{pmatrix} \frac{T_{21}}{T_{11}} & T_{22} - \frac{T_{21}T_{12}}{T_{11}} \\ \frac{1}{T_{11}} & -\frac{T_{12}}{T_{11}} \end{pmatrix} \tag{2.7}$$

where T_{11}, T_{12}, T_{21}, and T_{22} are the elements of the **T** matrix as evaluated from (2.6). The end-to-end transfer function is given by the S_{21} term of the overall **S** matrix divided by 2^N.

$$H(f) = \frac{S_{21}}{2^N} \cdot \frac{Z_{in}}{Z_{in} - Z_g} = \frac{1}{T_{11} \cdot 2^N} \cdot \frac{Z_{in}}{Z_{in} - Z_g}. \tag{2.8}$$

2.4.2 Typical Topology

We consider the simple MV topology of Figure 2.5 having three branches as described in [20]. The distance between the transmitter and the receiver is considered here to be 1000 m, and three indicative topologies are considered. Each of the corresponding line length parameters is given in Table 2.1 [20, 21]. The power line channel realizations in our simulation are depicted in Figure 2.6, which shows severe frequency selectivity.

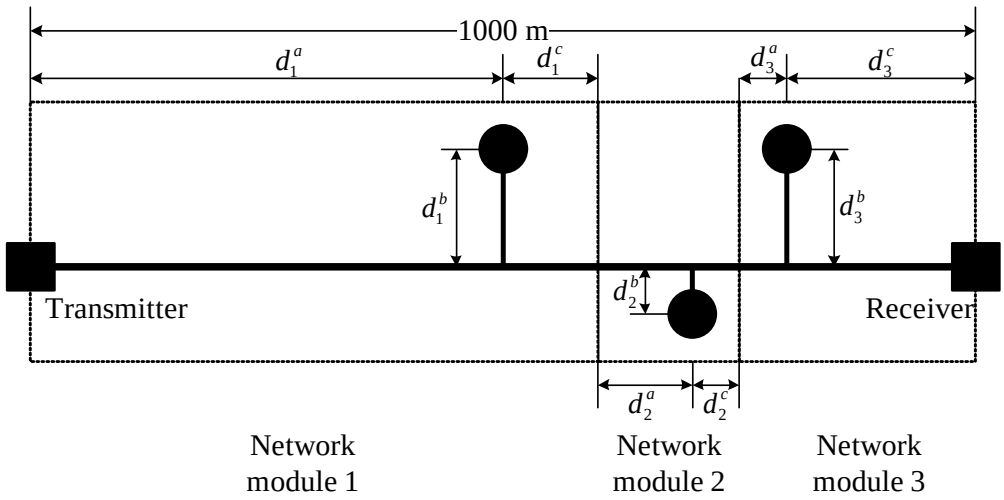

Figure 2.5: An example of the MV topology as a serial cascade of network modules.

Table 2.1: Description of Considered MV Topologies

Environment	Network Module	d_i^a[m]	d_i^b[m]	d_i^c[m]
Typical urban	L_1	500	6	100
	L_2	100	1	50
	L_3	50	6	200
Typical suburban	L_1	500	60	100
	L_2	100	10	50
	L_3	50	60	200
Typical rural	L_1	500	300	100
	L_2	100	150	50
	L_3	50	200	200

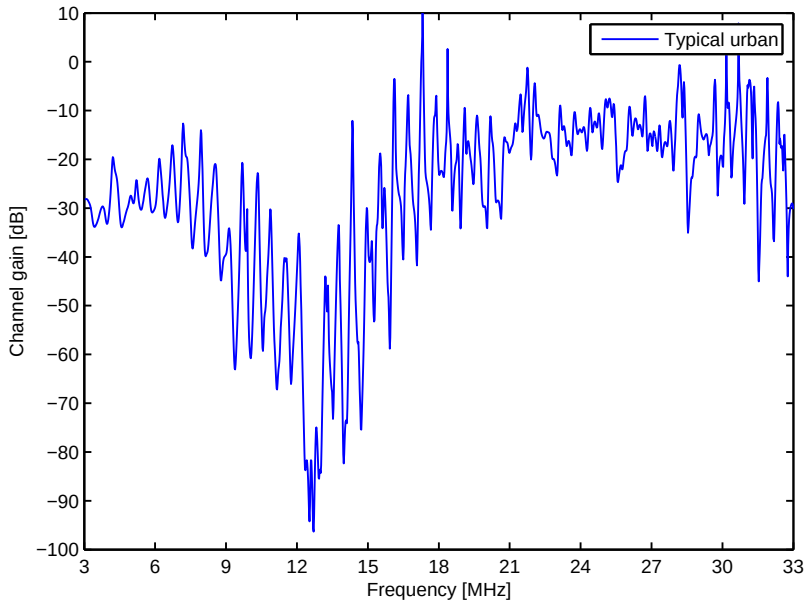

(a) Typical urban

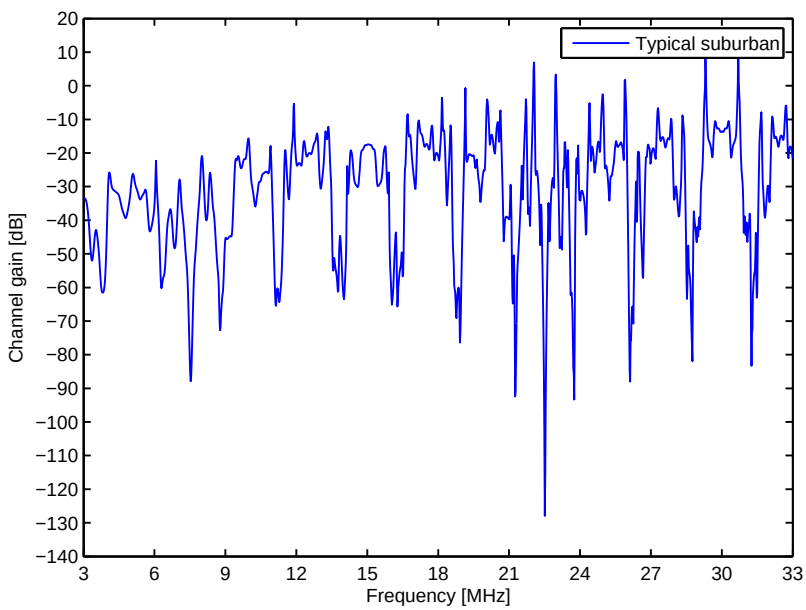

(b) Typical suburban (cont'd)

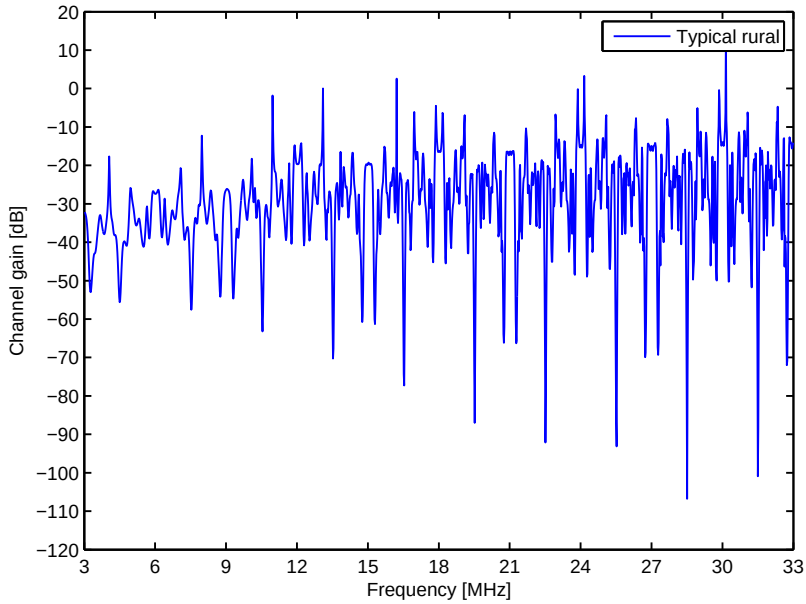

(c) Typical rural

Figure 2.6: Power line channel gain for the considered topologies.

2.5 MV Powerline Noise

In [22], a statistical approach to average colored background noise modeling is presented based on a large amount of noise measurements in MV, LV-Access and LV-In-Home situations. The results deliver some rule of thumb for determining an average noise level.

The noise power spectral density (PSD) of the model for MV is given by [22]

$$Z(f) = Z_0 + 37 \cdot \exp(-0.17 \times f\ [\text{MHz}])\ (\text{dBm/Hz}) \tag{2.9}$$

where Z_0 is the constant noise density.

Instead of fixed average value of $Z_0 = -105$ dBm/Hz in [22], we assume that Z_0 varies from -90 to -120 dBm/Hz, corresponding to the range from the worst to a moderate channel condition of PLC [23].

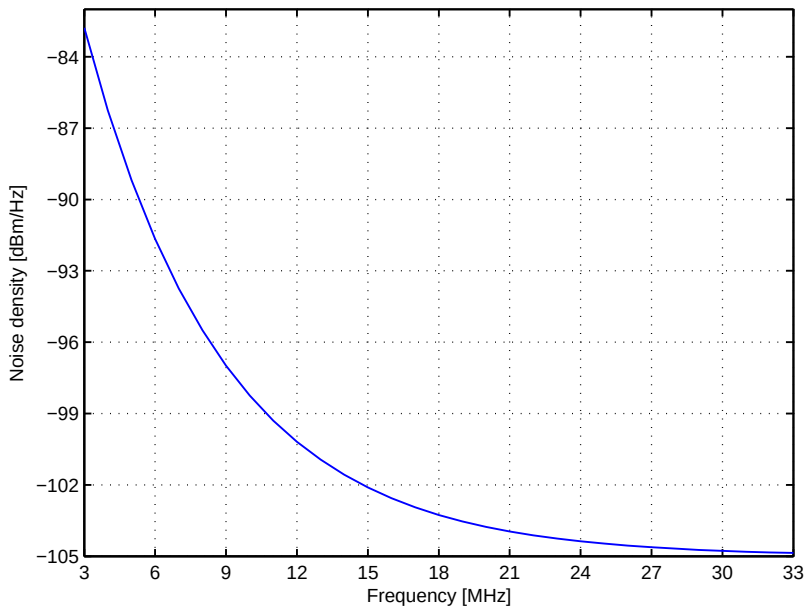

Figure 2.7: Powerline noise density for $Z_0 = -105$ dBm/Hz.

Figure 2.7 is the noise density when $Z_0 = -105$ (dBm/Hz), for the frequency range from 3 MHz to 33 MHz which is considered in the rest of the chapters. As shown in Equation. (2.9) and Figure 2.7, the noise floor is generally exponentially decreasing with increasing frequency. The exponential decrease with increasing frequency can be explained by the frequency dependent attenuation in cable networks and by the fact that the spectral density of most noise processes tend to decrease at higher frequencies.

Chapter 3

Optimal Subcarrier Pairing for Maximal Ratio Combining in OFDM Power Line Communications

3.1 Motivation

As discussed in previous chapters, power line communications (PLC) has been considered capable of playing a prominent role in the implementation of smart grids due to the inherent availability of power lines as carriers and the resulting advantages in terms of installation costs [24].

The reliability and robustness of the PLC network are prerequisite for providing appropriate services for Smart Grid. In communications, the studies of diversity schemes which seek to improve the reliability of the message signal by using two or more communication channels with different characteristics are dated back to several decades ago. In this work, we adopt a classical maximal ratio combining (MRC) diversity scheme for PLC to improve the reliability of the networks.

There have been various diversity approaches for PLC networks. In [25], both

space and frequency diversity in PLC was achieved by transmitting the same data symbol over two uncoupled pairs of wires and over two different carriers, thus improving the performance significantly compared to conventional single-wire OFDM systems. While previous work just implements antenna MRC to obtain spatial diversity gain in MIMO-OFDM PLC system, authors in [26, 27] proposed antenna & fading MRC scheme that effectively combines both multiple antenna and multipath fading diversity. In other study [28], a time-diversity permutation coding scheme combined with M-FSK modulation was proposed and the suitability of the scheme for a narrowband PLC system was presented. A cooperative relaying transmission protocol with multiple relay nodes for a MV power line channel was also presented [29]. By exploiting the cooperative diversity which comes from the combination of the relayed signal and the direct signal, a notable capacity increase was obtained.

The rest of this chapter is organized as follows. In Section 3.2, the system model for consideration is presented and the optimal sub-carrier pairing scheme is proposed. Section 3.3 shows numerical results to verify the performance enhancement of the proposed scheme, and the concluding remarks follow in Section 3.5. The notations used in this chapter are listed in Table 3.1.

3.2 Optimal Subcarrier Pairing for Maximal Ratio Combining

3.2.1 System Model

The received signal of the ith subcarrier is given as

$$y^{(i)} = H^{(i)}\sqrt{P}s^{(i)} + z^{(i)}, \tag{3.1}$$

where $s^{(i)}$ denotes the data symbol transmitted on the ith subcarrier with $\mathcal{E}\left\{\left|s^{(i)}\right|^2\right\} = 1$; $H^{(i)}$ is the complex channel gain between the transmitter and the receiver for the ith

Table 3.1: Summary of the notations used in Chapter 3

Notation	Definition
$y^{(i)}$	Received signal of the ith subcarrier
$H^{(i)}$	Channel gain of the ith subcarrier
$s^{(i)}$	Transmit symbol of the ith subcarrier
P	Transmit power of each subcarrier
$z^{(i)}$	Additive noise of the ith subcarrier
$Z^{(i)}$	Variance of the colored background noise of the ith subcarrier
$\gamma^{(i)}$	SNR of the ith subcarrier
$\mathcal{E}\{\cdot\}$	Expectation operator
$\lvert\cdot\rvert$	Magnitude of the signal, cardinality of the set
Γ^{tot}	The set of (the indices of) total subcarriers
Γ^{eff}	The set of (the indices of) subcarriers carrying effective data symbols
Γ^{MRC}	The set of (the indices of) subcarriers used for MRC
N^{tot}	The number of subcarriers of Γ^{tot}
N^{eff}	The number of subcarriers of Γ^{eff}
N^{MRC}	The number of subcarriers of Γ^{MRC}
$y_{\text{MRC}}^{(i,j)}$	Received signal after the MRC over the subcarrier pair (i, j)
$z_{\text{MRC}}^{(i,j)}$	Additive noise after the MRC over the subcarrier pair (i, j)
$\gamma_{\text{MRC}}^{(i,j)}$	SNR after the MRC over the subcarrier pair (i, j)

subcarrier; and $z^{(i)}$ is the additive noise imposed on the ith subcarrier. If we assume that the transmit power on each subcarrier is fixed to P and that the dominant noise term is only the colored background noise with variance of $Z^{(i)}$, the instantaneous received signal-to-noise-ratio (SNR)of the ith subcarrier can be denoted as

$$\gamma^{(i)} = \frac{|H^{(i)}|^2 P}{Z^{(i)}}. \tag{3.2}$$

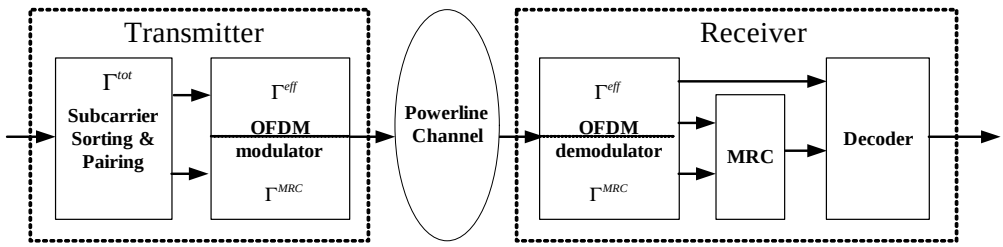

Figure 3.1: Block diagram of MRC diversity for OFDM power line communication.

Figure 3.1 describes the concept of MRC diversity in an OFDM PLC system. The set of total subcarriers of an OFDM system, Γ^{tot}, with cardinality of $|\Gamma^{\text{tot}}| = N^{\text{tot}}$ is split into the two sets of Γ^{eff} and Γ^{MRC} ($\Gamma^{\text{eff}} \cup \Gamma^{\text{MRC}} = \Gamma^{\text{tot}}$, $\Gamma^{\text{eff}} \cap \Gamma^{\text{MRC}} = \varnothing$). Γ^{eff} denotes the set of primary subcarriers for transmitting effective data symbols, which has cardinality of $\left|\Gamma^{\text{eff}}\right| = N^{\text{eff}}$, while the set of remaining subcarriers which can be used for MRC is denoted as Γ^{MRC} with cardinality of $\left|\Gamma^{\text{MRC}}\right| = N^{\text{MRC}} = N^{\text{tot}} - N^{\text{eff}}$.

For notational simplicity, the above sets of subcarriers also denote the sets of the indices of subcarriers. If the same data symbol s is transmitted over the pair of subcarriers (i, j) for MRC, where $i \in \Gamma^{\text{eff}}$ and $j \in \Gamma^{\text{MRC}}$, each of the received signals can be written similarly to (3.1). The maximal ratio combining is performed by multiplying each channel output with the complex-conjugate of the channel gain and inverse of the channel noise power [30]. Therefore, the resultant received signal after the MRC

process is denoted as

$$\begin{aligned} y_{\mathrm{MRC}}^{(i,j)} &= \frac{\sqrt{P}\left(H^{(i)}\right)^{*}}{Z^{(i)}} y^{(i)} + \frac{\sqrt{P}\left(H^{(j)}\right)^{*}}{Z^{(j)}} y^{(j)} \\ &= \left(\frac{|H^{(i)}|^2 P}{Z^{(i)}} + \frac{|H^{(j)}|^2 P}{Z^{(j)}} \right) s + z_{\mathrm{MRC}}^{(i,j)}, \end{aligned} \tag{3.3}$$

where $*$ denotes the complex conjugation and where

$$z_{\mathrm{MRC}}^{(i,j)} = \frac{\sqrt{P}\left(H^{(i)}\right)^{*}}{Z^{(i)}} z^{(i)} + \frac{\sqrt{P}\left(H^{(j)}\right)^{*}}{Z^{(j)}} z^{(j)}. \tag{3.4}$$

3.2.2 Optimal Subcarrier Pairing

The received SNR after the MRC of the *i*th and *j*th subcarrier is the sum of each SNR per subcarrier in linear scale,

$$\gamma_{\mathrm{MRC}}^{(i,j)} = \gamma^{(i)} + \gamma^{(j)}, \tag{3.5}$$

and the achievable data rate can be computed as

$$R^{(i,j)} = \log_2(1 + \gamma_{\mathrm{MRC}}^{(i,j)}) \Delta f, \tag{3.6}$$

where Δf denotes the subcarrier spacing, $i \in \Gamma^{\mathrm{eff}}$, and $j \in \Gamma^{\mathrm{MRC}}$. Obviously, a different subcarrier pairing combination (i, j) results in a different SNR gain by MRC, which translates into a different achievable data rate. Here, we consider which subcarrier pairing combination is optimal for maximizing the overall data rate $R^{\mathrm{tot}} = \sum_{(i,j)} R^{(i,j)}$.

Let us start with the following inequality,

$$\begin{aligned} &\log_2(a_1 + \Delta_2) - \log_2(a_1 + \Delta_1) > \\ &\qquad \log_2(a_2 + \Delta_2) - \log_2(a_2 + \Delta_1) \end{aligned} \tag{3.7}$$

for all $0 < a_1 < a_2$ and $0 < \Delta_1 < \Delta_2$. Note that the logarithmic function is monotonically increasing, whereas the rate of change over a given interval is monotonically decreasing. For arbitrary subcarriers $i, i' \in \Gamma^{\mathrm{eff}}$ and $j, j' \in \Gamma^{\mathrm{MRC}}$ with their respective SNRs

of $\gamma^{(i)} < \gamma^{(i')}$ and $\gamma^{(j)} < \gamma^{(j')}$, if we substitute $a_1 = 1+\gamma^{(i)}$, $a_2 = 1+\gamma^{(i')}$, $\Delta_1 = \gamma^{(j)}$ and $\Delta_2 = \gamma^{(j')}$, the following inequality holds:

$$\begin{aligned} &\log_2(1+\gamma^{(i)}+\gamma^{(j')}) - \log_2(1+\gamma^{(i)}+\gamma^{(j)}) \\ &\quad > \log_2(1+\gamma^{(i')}+\gamma^{(j')}) - \log_2(1+\gamma^{(i')}+\gamma^{(j)}) \\ &\Leftrightarrow \log_2(1+\gamma^{(i,j')}) + \log_2(1+\gamma^{(i',j)}) \\ &\quad > \log_2(1+\gamma^{(i,j)}) + \log_2(1+\gamma^{(i',j')}). \end{aligned} \tag{3.8}$$

This implies that in order to achieve a gain in the data rate through MRC, the subcarrier with the lower SNR in Γ^{eff} should be paired with the subcarrier with the higher SNR in Γ^{MRC}. [1]

When the data symbols are transmitted only over the set of primary subcarriers without performing MRC, it is reasonable to use the best N^{eff} of N^{tot} subcarriers in terms of the SNR intuitively. Therefore, the total subcarriers are sorted in a descending order of their SNRs, which yields the sorted subcarrier indices $\{\alpha_1, \ldots, \alpha_{N^{\text{eff}}}, \ldots, \alpha_{N^{\text{tot}}}\}$, after which we set $\Gamma^{\text{eff}} = \{\alpha_1, \ldots, \alpha_{N^{\text{eff}}}\}$ and $\Gamma^{\text{MRC}} = \{\alpha_{N^{\text{eff}}+1}, \ldots, \alpha_{N^{\text{tot}}}\}$. It is assumed that N^{MRC} cannot be larger than N^{eff} due to spectral efficiency; hence, the first $N^{\text{eff}} - N^{\text{MRC}}$ of the sorted subcarriers may be transmitted without MRC diversity. Rewriting the elements of Γ^{MRC} as $\alpha_{N^{\text{eff}}+1} = \beta_1, \ldots, \alpha_{N^{\text{tot}}} = \beta_{N^{\text{MRC}}}$, we obtain the optimal subcarrier pairing of $(\alpha_{N^{\text{eff}}}, \beta_1)$, $(\alpha_{N^{\text{eff}}-1}, \beta_2)$, …, $(\alpha_{N^{\text{eff}}-N^{\text{MRC}}+1}, \beta_{N^{\text{MRC}}})$. The overall procedures are summarized as follows.

Optimal subcarrier pairing procedure

After the transmitter acquires the CSI,

[1] The term '*subcarrier pairing*' has been widely used for studies of OFDM relay system in which a transmission is completed in two time slots [31, 32]. The subcarrier pairing result for the considered system is somewhat different from that for OFDM relay system, where, with the objective of maximizing sum rate under a total power constraint, the strongest source-to-relay subcarrier should be paired with the strongest relay-to-destination subcarrier [32].

1) Sort the total subcarriers $\{\alpha_1, \ldots, \alpha_{N^{\text{eff}}}, \ldots, \alpha_{N^{\text{tot}}}\}$ in a descending order of their SNRs, where $\alpha_1 > \cdots > \alpha_{N^{\text{eff}}} > \cdots > \alpha_{N^{\text{tot}}}$. [2]

2) According to some criterion, divide the sorted subcarrier set into $\Gamma^{\text{eff}} = \{\alpha_1, \ldots, \alpha_{N^{\text{eff}}}\}$ and $\Gamma^{\text{MRC}} = \{\beta_1, \ldots, \beta_{N^{\text{MRC}}}\}$ with the constraint of $N_{\text{eff}} + N_{\text{MRC}} = N_{\text{tot}}$, where $\{\beta_j\} = \{\alpha_{N^{\text{eff}}+j}\}$ for $j = 1, \ldots, N_{\text{MRC}}$, therefore $\alpha_{N^{\text{eff}}} < \alpha_{N^{\text{eff}}-1} < \cdots < \alpha_1$ and $\beta_1 > \beta_2 > \cdots > \beta_{N^{\text{MRC}}}$.

3) If $N_{\text{eff}} \geq N_{\text{MRC}}$, go to step 3a); else if $N_{\text{eff}} < N_{\text{MRC}}$, go to step 3b).

   3a) Transmits the signal for diversity over the subcarrier pair of $(\alpha_{N^{\text{eff}}-j+1}, \beta_j)$ for $j = 1, \ldots, N_{\text{MRC}}$, and transmits without diversity over remaining subcarriers $\{\alpha_1, \ldots, \alpha_{N^{\text{eff}}-N^{\text{MRC}}}\}$

   3b) Transmits the signal for diversity over the subcarrier pair of $(\alpha_i, \beta_{N^{\text{eff}}-i+1})$ for $i = 1, \ldots, N_{\text{eff}}$, and remaining subcarriers $\{\beta_{N^{\text{MRC}}-N^{\text{eff}}}, \ldots, \beta_{N^{\text{MRC}}}\}$ are not used for transmission.

3.3 Numerical Results

3.3.1 Simulation Environments

In this section, the symbol error rate (SER) performances are evaluated by Monte Carlo simulation. We consider a power line OFDM system compatible with the DS2/UPA PHY specification [33]. The OFDM symbol uses 1536 subcarriers, which occupy a total bandwidth of 30 MHz from 3 to 33 MHz with a subcarrier spacing Δf of 19.5312 kHz. OFDM parameters for simulation are presented in Table 3.2. The maximum injected power spectral density (IPSD) is limited by -60 dBm/Hz for 3–30 MHz

[2] For simplicity, we abuse notation slightly by referring the symbol with braces or parentheses such as $\{\alpha_i\}, (\alpha_i, \beta_j)$ to the sorted subcarrier index itself, and referring the symbol without those to the SNR of corresponding index.

and -74 dBm/Hz for 30–33 MHz [20]. For simplicity, simulations are run below 30 MHz with constant IPSD of -60 dBm/Hz, thus the total number of subcarriers is $N^{\text{tot}} = 1382$.

Table 3.2: OFDM parameters for simulation in Chapter 3

Parameter	Value
FFT size	2048
Sampling clock	40 [MHz]
OFDM subcarrier spacing, Δf	19.5312 [kHz]
useful OFDM symbol duration, $1/\Delta f$	51.2 [μs]
Cyclic prefix	20 [μs]
Total number of used subcarriers, N^{tot}	1382
Occupied bandwidth	3 – 30 [MHz]

It is known that the impulsive noise, which is one of the major impairments of PLC transmission in the time domain, can be properly mitigated by an existing cancellation scheme, as assessed in earlier work [34]. Therefore, we assume that the signals are mainly corrupted by colored background noise only. Moreover, the colored background noise vary slowly over time [13, 35], i.e., the transfer function of PLC channel can be considered quasi-static [36]. In this case, channel state information (CSI) exchange between the receiver and the transmitter need not occur frequently, so the overhead burden of CSI feedback is not significant.

According to the colored noise model of (2.9), the variance of the noise of the ith subcarrier can be represented as

$$Z^{(i)} = Z_0 + 37\exp[-0.17 \times 10^{-6}(f_L + \Delta f \cdot i)] \text{ (dBm/Hz)} \tag{3.9}$$

Here, f_L is the lowest frequency, which corresponds to 3×10^6 Hz for the considered system; and i is the subcarrier index.

Two different MV topologies (a typical urban and a typical rural topology) are considered for the simulation. To ensure the proposed pairing scheme is meaningful in real environments, the independence between pair of subcarriers should be verified, and this is briefly discussed in Appendices.

3.3.2 SER Performance Analysis

There is a tradeoff between the spectral efficiency and the MRC gain with respect to the number of subcarriers for MRC. Here, we simply assume that one half of all subcarriers are utilized for MRC. Accordingly, all data symbols are transmitted exactly twice in the frequency domain. It is also assumed that every subcarrier is modulated with the same constellation order. Figure 3.2 shows the simulation results of the proposed optimal subcarrier pairing scheme as well as other transmit schemes for comparison. First, as a reference, we evaluate the performance for the case in which all of the subcarriers are used for transmission without MRC diversity ('*all subcarriers*' case). In this case, the portion of subcarriers with poor channel quality is high; For instance, when $Z_0 = -92$ dBm/Hz, the SNRs of about half of the subcarriers are smaller than 0 dB. As a result, a very high symbol error rate larger than 10^{-1} is shown. By selecting, for transmission, the best half of the subcarriers with respect to the SNR ('*sorted subcarriers*' case), noticeable improvements in the SER performance are observed for the expense of a loss of spectral efficiency. Due to the use of half of the subcarriers, the total transmit power compared to the former case is halved. Thus, the transmit power for each subcarrier can be doubled theoretically but cannot be realized practically due to the IPSD limitation for PLC. The simulation results for this theoretical case are also depicted ('*doubled power*' case).

Next, a case in which the remaining subcarriers are used for MRC is considered. If the primary subcarriers are paired with the remaining subcarriers for MRC randomly ('*random pairing*' case), the performance gain from MRC is very small. By

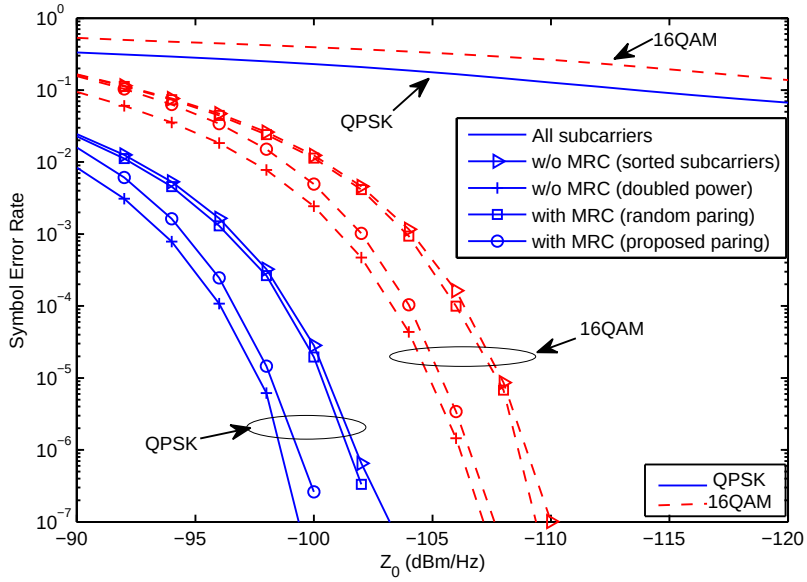

(a)

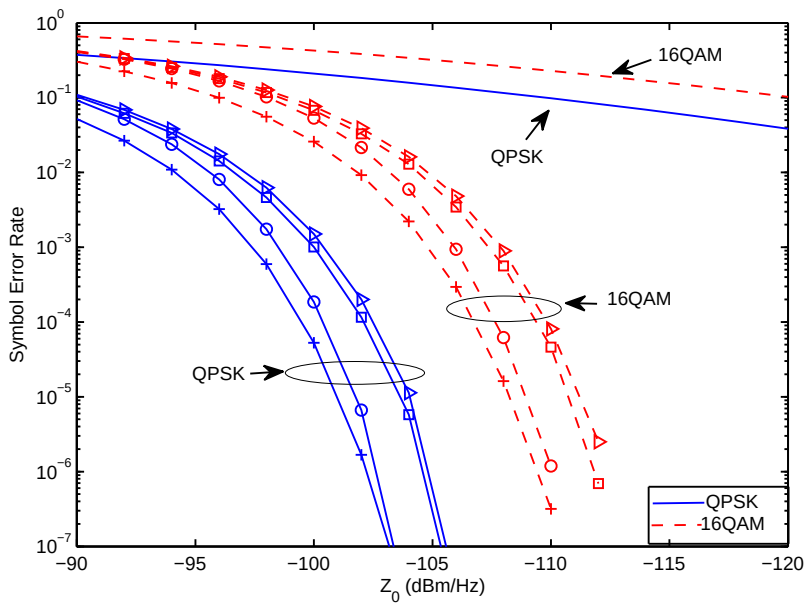

(b)

Figure 3.2: Symbol error rate (SER) performance as a function of constant noise density for (a) typical urban MV topology and (b) typical rural MV topology.

utilizing the subcarriers for MRC according to the proposed optimal pairing scheme (‘*optimal pairing*’ case), it is noted that the SER performance is improved significantly compared to the case without MRC. It is also shown that the performance approaches quite closely to the theoretical case of doubling the power.

Regardless of the modulation order or the PLC network topology, the performance gain from optimal subcarrier paring increases dramatically as the channel conditions improve. For example, in a typical urban environment with 16-QAM modulation, the SER performance with the proposed scheme compared to the case without MRC is improved about 10 % when $Z_0 = -92$ dBm/Hz, whereas it is improved by orders of magnitude when $Z_0 = -104$ dBm/Hz.

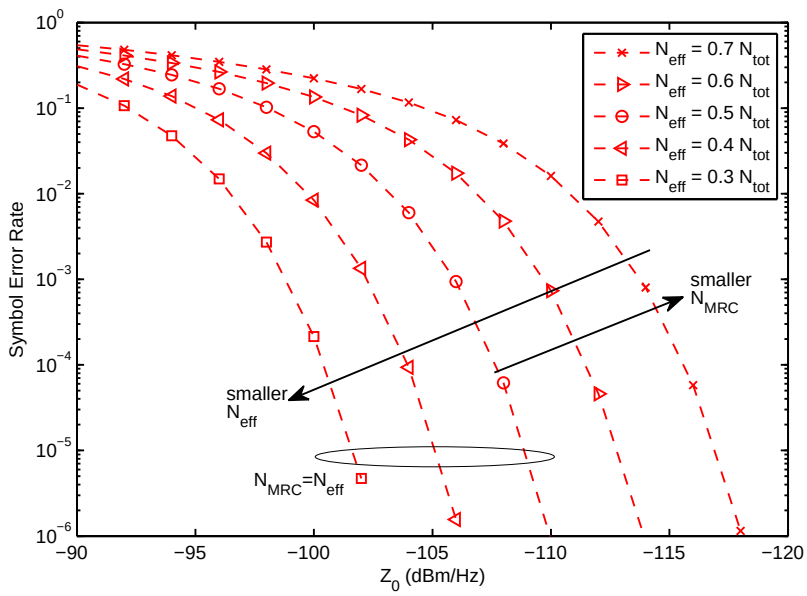

Figure 3.3: SER performance variation of optimal pairing scheme with respect to the ratio of N_{eff} (N_{MRC}) to N_{tot} for typical rural MV topology, 16-QAM modulation.

In previous results, we chose $N_{\text{eff}} = N_{\text{MRC}} = \frac{1}{2}N_{\text{tot}}$ so that all effective data subcarriers are combined with remaining subcarriers for diversity. In this case, the number of diversity subcarriers is maximum according to the proposed paring scheme. We

observe that how the ratio of the number of effective data subcarriers (and/or corresponding the number of diversity subcarriers) to the number of total subcarriers affects the SER performance. Figure 3.3 is the simulation results for typical rural MV topology and 16-QAM modulation by varying the ratio $\frac{N_{\text{eff}}}{N_{\text{tot}}}$. When $\frac{N_{\text{eff}}}{N_{\text{tot}}} > 0.5$, the subcarriers for diversity are smaller and have lower SNR in average sense relative to the reference case with $\frac{N_{\text{eff}}}{N_{\text{tot}}} = 0.5$, so the SER performances are degraded. On the contrary, when $\frac{N_{\text{eff}}}{N_{\text{tot}}} < 0.5$, the SER performances are improved because the effective data subcarriers and diversity subcarriers have higher SNR in average sense relative to the reference case and subcarriers with lower SNR are not used for transmission.

3.3.3 Performance Comparison with Equal Gain Combining

To identify the applicability of the proposed scheme to other combining techniques, equal gain combining (EGC) is considered. While two signals are added with the weights proportional to the received SNR in MRC diversity, two signals are added with the weights which have equal amplitudes in EGC diversity [30]. But in both combining techniques, co-phasing reception of individual symbols is preceded to the addition of two signals. The EGC in colored noise circumstances can be performed as follows:

$$\begin{aligned} y_{\text{EGC}}^{(i,j)} &= \frac{1}{\sqrt{Z^{(i)}}} \frac{\left(H^{(i)}\right)^*}{\left|H^{(i)}\right|} y^{(i)} + \frac{1}{\sqrt{Z^{(j)}}} \frac{\left(h^{(j)}\right)^*}{\left|h^{(j)}\right|} y^{(j)} \\ &= \left(\frac{\left|H^{(i)}\right|}{\sqrt{Z^{(i)}}} + \frac{\left|h^{(j)}\right|}{\sqrt{Z^{(j)}}} \right) \sqrt{P} s + z_{\text{EGC}}^{(i,j)}, \end{aligned} \tag{3.10}$$

where

$$z_{\text{EGC}}^{(i,j)} = \frac{1}{\sqrt{Z^{(i)}}} \frac{\left(H^{(i)}\right)^*}{\left|H^{(i)}\right|} z^{(i)} + \frac{1}{\sqrt{Z^{(j)}}} \frac{\left(h^{(j)}\right)^*}{\left|h^{(j)}\right|} z^{(j)}. \tag{3.11}$$

Fig 3.4 shows the performance difference between two combining schemes with respect to the pairing algorithm. The simulation results confirm the theory in which the performance of EGC is poorer than MRC [30]. The performance gap between EGC and MRC is quite large for the random pairing cases in contrast to negligible difference

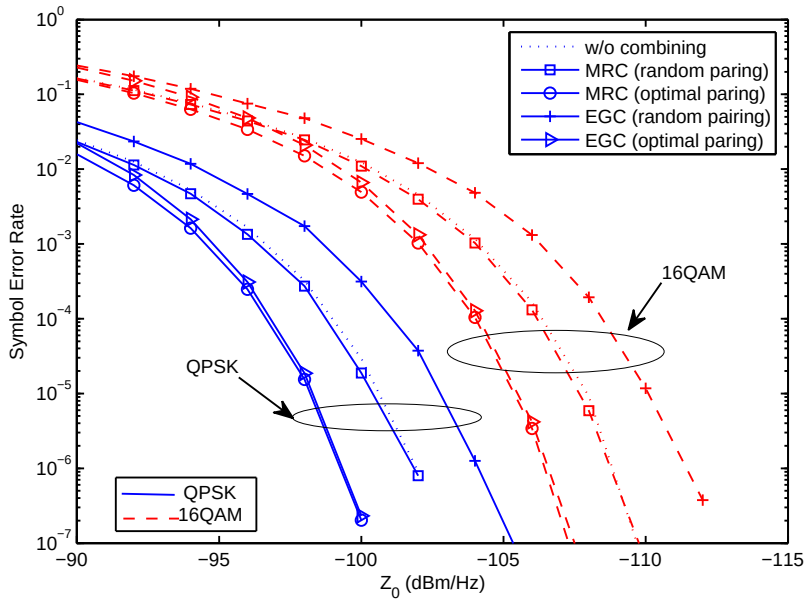

(a)

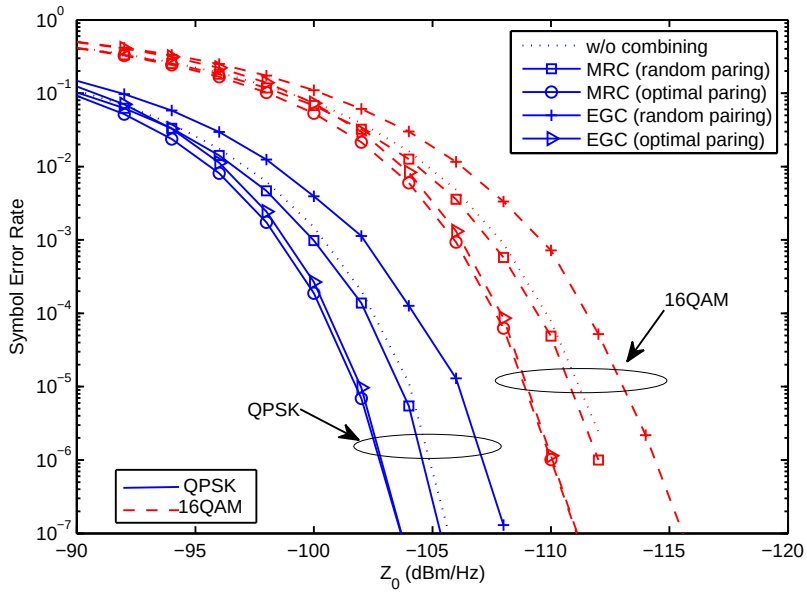

(b)

Figure 3.4: Performance comparison between MRC and EGC for (a) typical urban MV topology and (b) typical rural MV topology.

for the optimal pairing cases. Moreover, considering the random pairing cases, the performance of EGC is much worse than the case where the diversity combining is not used but only transmits on the best SNR subcarriers (the dotted line graphs). It is different from the MRC case in which shows the small diversity gain over the same case in spite of random pairing. When the EGC is used for combining techniques, the proposed optimal pairing algorithm provides diversity gain almost equally in MRC case, but the random pairing rather degrades the performance. This means that in order to obtain the diversity gain regardless of the combining techniques, the auxiliary subcarriers for diversity with the low SNR should be paired according to the proposed scheme.

3.4 Precoding Scheme to Compensate Spectral Loss Due to Diversity Transmission

The proposed subcarrier pairing scheme with MRC achieved the diversity gain in terms of SER, but, in return, made inherent spectral loss due to the transmission of same data symbol twice over subcarrier pair. Wireless systems using multiple antennas can provide two types of gains: diversity gain and spatial multiplexing gain. Both gains can be simultaneously obtained, but there is a fundamental tradeoff how much of each type of gain any coding scheme can extract [37]. Many approaches have been studied to achieve both gains optimally. With the motivation to compensate the spectral loss due to diversity transmission of subcarrier pairing, we adopt a precoding scheme [38] proposed for wireless MIMO system and apply to OFDM PLC system.

3.4.1 Review of the Minimum Distance-Based Precoder for MIMO Spatial Multiplexing Systems

In wireless communications, the multiple-input multiple output (MIMO) systems can improve the reliability or the data rate significantly in comparison with single-input single-output (SISO) systems. Some precoding schemes are needed to achieve the capacity gain through the use of multiple antennas. It is shown that in [39] the capacity-achieving approach is to access the eigenmodes of the channel matrix through a singular value decomposition (SVD) and transmit independent complex Gaussian symbols over each eigenmode with appropriate power allocation. With the assumption of having the channel state information(CSI) at the transmitter side, the optimal power allocation can be obtained by applying the classical waterfilling (WF) technique. The WF solution is based on the criterion which maximizes the output capacity. Other criteria such as beamforming, minimum mean square error (MMSE), quality of service (QoS), or maximization of the minimum eigenvalue (max-$\lambda_{\min}$) can lead different design of linear precoders. These solutions lead to power allocation with diagonal solutions based on the SVD [41].

In practice, discrete QAM-like constellations are used for transmission, so above technique with the assumption of Gaussian inputs is no longer optimal [42]. In [38], the authors proposed a linear precoding scheme which maximizes the criterion on the minimum Euclidean distance $d_{\min}$ between symbol points at the receiver side with BPSK or QPSK constellations. Contrary to the above solutions, this approach leads to a nondiagonal precoder.

3.4.2 Optimal Minimum Distance-Based Precoder for QPSK Constellation

Authors in [38] considered a MIMO system with n_R receive and n_T transmit antennas for achieving b independent data streams. Assuming a quasi-static flat-fading channel

model, the received signal is given by

$$\mathbf{y} = \mathbf{GHFs} + \mathbf{G}\nu \tag{3.12}$$

where $\mathbf{y}$ is the $b \times 1$ received symbol vector, $\mathbf{H}$ is the $n_R \times n_T$ channel matrix, $\mathbf{F}$ is the $n_T \times b$ linear precoder matrix, $\mathbf{G}$ is the $b \times n_R$ linear decoder matrix, $\mathbf{s}$ is the $b \times 1$ transmitted symbol vector, and ν is the zero-mean $n_R \times 1$ additive noise vector. It is assumed that $b \leq r = \text{rank}(\mathbf{H}) \leq \min(n_T, n_R)$ and $\mathcal{E}\{\mathbf{ss}^\dagger\} = \mathbf{I}_b$, $\mathcal{E}\{\mathbf{s}\nu^\dagger\} = \mathbf{0}$ and $\mathcal{E}\{\nu\nu^\dagger\} = \mathbf{R}$ with $\mathbf{R}$ the noise covariance matrix, where $\dagger$ represents the complex conjugate transpose. By performing virtual transformation, a diagonalized channel matrix and a whitened noise can be obtained. With the following decompositions $\mathbf{F} = \mathbf{F}_v\mathbf{F}_D$ and $\mathbf{G} = \mathbf{G}_v\mathbf{G}_D$, (3.12) can be re-expressed as

$$\mathbf{y} = \mathbf{G}_D\mathbf{H}_v\mathbf{F}_D\mathbf{s} + \mathbf{G}_D\nu_v \tag{3.13}$$

where $\mathbf{H}_v = \mathbf{G}_v\mathbf{HF}_v$ is the $b \times b$ virtual channel matrix, and $\nu_v = \mathbf{G}_v\nu$ is the $b \times 1$ virtual noise vector. The unitary matrices $\mathbf{G}_v$ and $\mathbf{F}_v$ are chosen so as to whiten the noise, diagonalize the channel, and reduce dimension to b. The virtual channel matrix $\mathbf{F}_v$ is denoted as

$$\mathbf{H}_v = \text{diag}(\sigma_1, \sigma_2, \ldots, \sigma_b) \tag{3.14}$$

where σ_k for $k = 1, \ldots, b$ stands for kth virtual subchannel gain (sorted by decreasing order).

The precoder matrix $\mathbf{F}_D$ that maximizes the minimum Euclidean distance $d_{\min}$ of the received constellation under the power constraint $\text{trace}(\mathbf{FF}^\dagger) = p_0$ are determined. The $d_{\min}$ is defined by

$$d_{\min}(\mathbf{F}_D) = \min_{(\mathbf{s}_k, \mathbf{s}_l), \mathbf{s}_k \neq \mathbf{s}_l} \|\mathbf{H}_v\mathbf{F}_D(\mathbf{s}_k - \mathbf{s}_l)\| \tag{3.15}$$

where $\mathbf{s}_k$ and $\mathbf{s}_l$ are two symbols vectors whose entries are elements of $\mathcal{C}$. Then, the max-$d_{\min}$ precoder is the solution of

$$\mathbf{F}_D^{d_{\min}} = \arg\max_{\mathbf{F}_D} d_{\min}(\mathbf{F}_D) \tag{3.16}$$

under the above power constraint.

Due to the difficulty of determining of the precoding matrix $\mathbf{F}_D$, the authors in [38] only considered for two independent data streams, $b = 2$. In this case, the virtual channel matrix can be parameterized as follows:

$$\mathbf{H}_v = \begin{pmatrix} \sigma_1 & 0 \\ 0 & \sigma_2 \end{pmatrix} = \rho \begin{pmatrix} \cos\gamma & 0 \\ 0 & \sin\gamma \end{pmatrix} \tag{3.17}$$

where $\rho = \sqrt{\rho_1^2 + \rho_2^2}$ is a positive real parameters related to the eigen-channel gain, and $\gamma = \arctan\frac{\sigma_2}{\sigma_1}$ is an angle linked to the singular values ratio and meeting $\sigma_1 \geq \sigma_2 > 0$, *i.e.*, $0 < \gamma \leq \pi/4$.

The precoder matrix can be simplified as follows [38]:

$$\mathbf{F}_D = \sqrt{p_0} \begin{pmatrix} \cos\psi & 0 \\ 0 & \sin\psi \end{pmatrix} \begin{pmatrix} \cos\theta & \sin\theta \\ -\sin\theta & \cos\theta \end{pmatrix} \begin{pmatrix} 1 & 0 \\ 0 & e^{j\phi} \end{pmatrix} \tag{3.18}$$

The angles θ and ϕ correspond to scaling and rotation of the received constellation, respectively.

It was shown in [38] that the optimal solution for QPSK modulation gives two precoder expressions

i) $0 \leq \gamma \leq \gamma_0$

$$\mathbf{F}_D^{d_{\min}} = \mathbf{F}_{r1} = \sqrt{p_0} \begin{pmatrix} \sqrt{\frac{3+\sqrt{3}}{6}} & \sqrt{\frac{3+\sqrt{3}}{6}} e^{j\pi/12} \\ 0 & 0 \end{pmatrix} \tag{3.19}$$

ii) $\gamma_0 \leq \gamma \leq \pi/4$

$$\mathbf{F}_D^{d_{\min}} = \mathbf{F}_{octa} = \sqrt{\frac{p_0}{2}} \begin{pmatrix} \cos\psi & 0 \\ 0 & \cos\psi \end{pmatrix} \begin{pmatrix} 1 & e^{j\frac{\pi}{4}} \\ -1 & e^{j\frac{\pi}{4}} \end{pmatrix} \tag{3.20}$$

$$\text{where } \begin{cases} \psi = \arctan\frac{\sqrt{2}-1}{\cos\gamma} \\ \gamma_0 = \arctan\sqrt{\frac{3\sqrt{3}-2\sqrt{6}+2\sqrt{2}-3}{3+\sqrt{3}-2\sqrt{6}+1}} \simeq 17.28^\circ. \end{cases} \tag{3.21}$$

The parameter ψ is related to the power allocation, and the constant threshold γ_0 permits the precoder to use one or two eigen-subchannels.

3.4.3 Application to PLC OFDM System

Previous precoding scheme can be applied to an OFDM system with N subcarriers having their channel gains $\{h_k\}_{k=1}^{N}$. We consider that two subcarriers comprise 2×2 diagonal channel matrix. The N subcarriers are first grouped into $N/2$ pairs, then, from the $N/2$ independent transmissions,

$$\mathbf{y}_k = \mathbf{G}_k \tilde{\mathbf{H}}_k \mathbf{F}_k \mathbf{s}_k + \mathbf{G}_k \boldsymbol{\nu}_k, \;\; 1 \leq k \leq N/2, \tag{3.22}$$

$N/2$ precoders $\{\mathbf{F}_k\}_{k=1}^{N/2}$ are constructed. The pairing used in [40] is to combine the strongest subcarrier with the weakest subcarrier, the second strongest with the second weakest etc. This is similar to the pairing scheme for MRC in previous chapters, where the subcarriers are sorted according not to the channel gain but the SNR. If the average noise density is constant for all subcarriers (white noise), two sorting criteria give equivalent results, but different results for colored noise in PLC. Precoding with both sorting schemes are considered for performance evaluation, where the former approach based on the channel gain only is referred as *scheme I*, the latter approach based on SNR with the consideration of noise statistics is referred as *scheme II*. Let $\{\tilde{h}_1, \tilde{h}_2, \ldots \tilde{h}_N\}$ denote the sorted subcarriers set according to either sorting criterion, then the channel matrix for each pair is given by

$$\tilde{\mathbf{H}}_k = \begin{pmatrix} \tilde{h}_k & 0 \\ 0 & \tilde{h}_{k-N+1} \end{pmatrix} \tag{3.23}$$

Power constraint for each precoder is $p_0 = 2P_{sub}$, where P_{sub} is the transmit power of each subcarrier with IPSD limit for PLC.

3.4.4 Performance Comparison of max-$d_{\min}$ Precoder for QPSK Modulation

Simulations are performed under the same parameters in Chapter 3. Figure 3.5 shows the SER performances considering the precoding scheme for QPSK modulation pre-

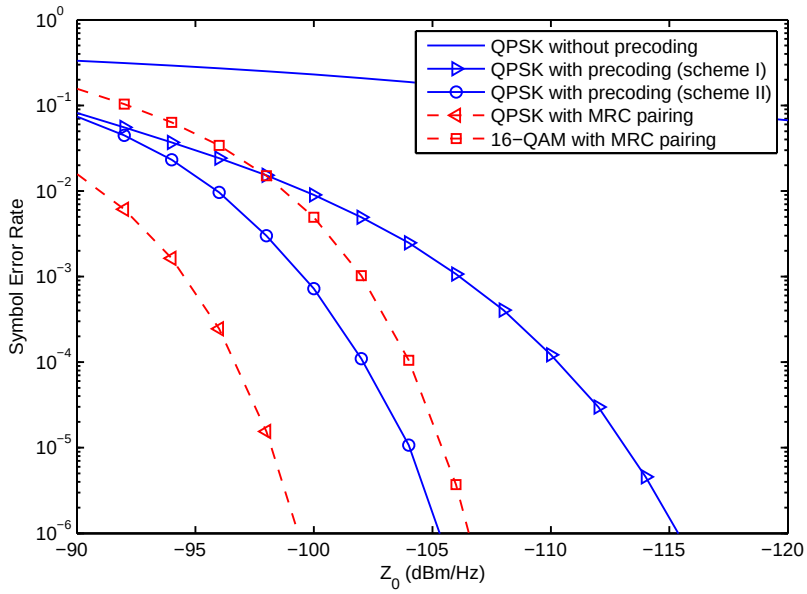

(a)

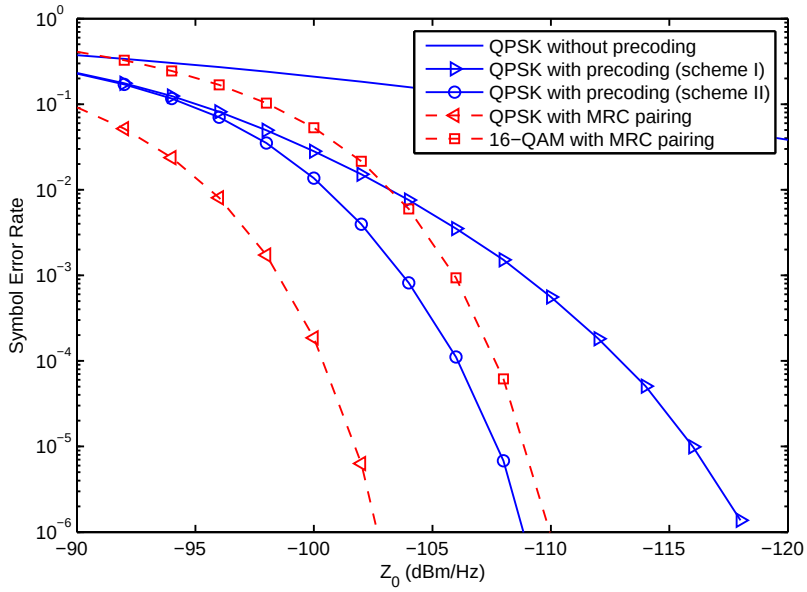

(b)

Figure 3.5: Symbol error rate (SER) performance of precoding scheme for QPSK modulation in (a) typical urban MV topology and (b) typical rural MV topology.

sented in previous section. For comparison, performances of MRC with optimal subcarrier pairing scheme proposed in Chapter 3 also represented. As shown in figures, by applying precoding scheme for transmission, significant performance improvements are achieved compared to the no precoding case, and the improvement, especially, is more pronounced for the precoding scheme II case. This improvement comes at the expense of increased complexity of transceivers which require the determination of precoders and more complex ML reception.

As expected, for same QPSK modulation, MRC with subcarrier pairing scheme outperforms in terms of SER due to the diversity by transmitting same data symbol twice. To consider the same spectral efficiency at the transmitter, the performance of MRC pairing for 16-QAM modulation case should be compared. The 16-QAM with MRC pairing scheme always shows some performance degradation compared to the QPSK with precoding scheme II case. However, as for PLC noise density decreases, 16-QAM with MRC pairing scheme outperforms the QPSK with precoding scheme I case.

To compare more realistic throughput performance, we adopt simple convolutional channel coding with code rate 1/2 for transmission. Simulations are performed in very noisy channel for $Z_0 = -90 \sim -100$ dBm/Hz. The performance of coded bit error rate (BER) is shown in Figure 3.6. If we think the x-axis as SNR-related parameter such $\frac{E_b}{N_0}$, then, for a given target BER, the difference between the graph of two different scheme can be interpreted as precoding gain. That is, when target BER is equal to 10^{-3}, optimal max-$d_{\min}$ precoder (scheme II) gives precoding gain about 2.5 dB for typical urban case and about 3 dB for typical rural case compared to the MRC pairing scheme with higher modulation which yields same spectral efficiency.

Figure 3.7 is the average throughput actually achieved. As shown in figure, when the PLC channel very harsh, the precoding scheme always outperforms the MRC pairing scheme with higher modulation in terms of average throughput. But as the channel

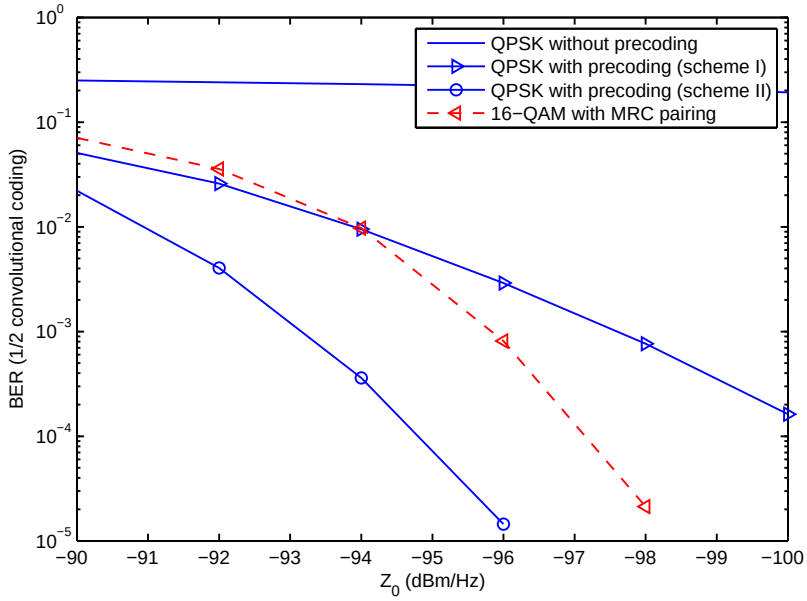

(a)

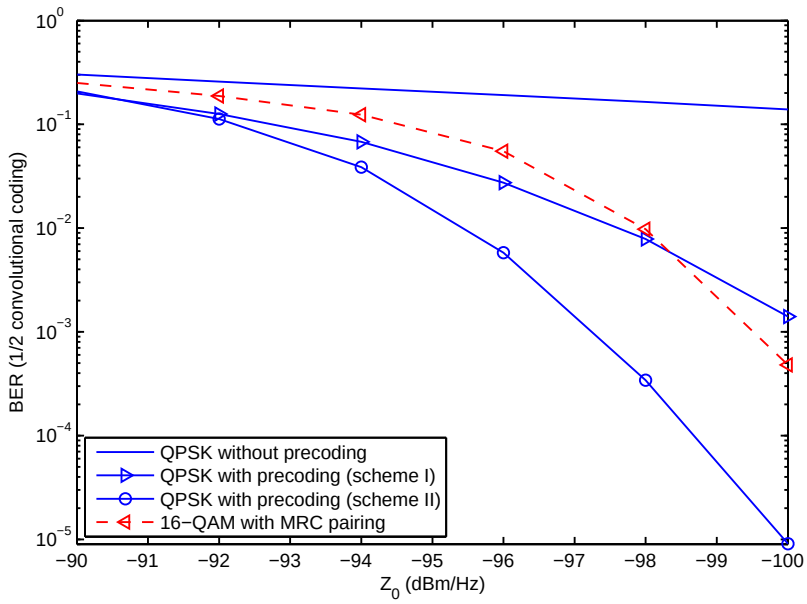

(b)

Figure 3.6: Bit error rate (BER) performance of precoding scheme for QPSK modulation with 1/2 convolutional coding in (a) typical urban MV topology and (b) typical rural MV topology.

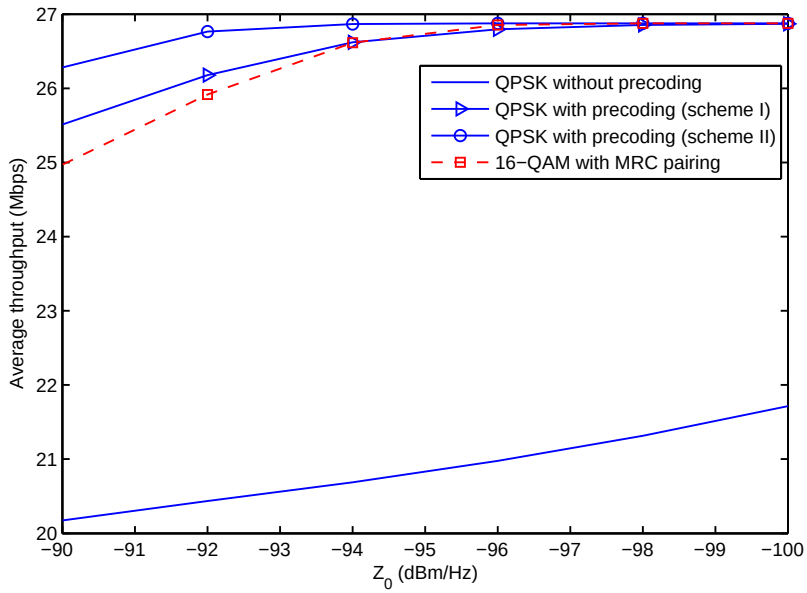

(a)

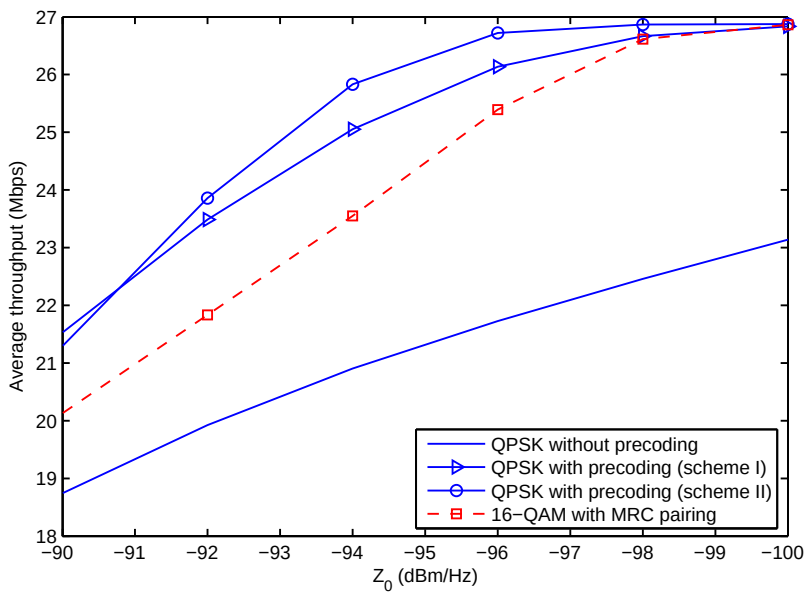

(b)

Figure 3.7: Average throughput performance of precoding scheme for QPSK modulation in (a) typical urban MV topology and (b) typical rural MV topology.

environment is getting better slightly, the difference of the achieved throughput via the precoding scheme and the MRC pairing scheme is getting smaller steeply. This means that it is better to use the MRC diversity pairing scheme with higher modulation than the max-$d_{\min}$ precoding scheme except for extremely noisy environments.

3.4.5 Performance Comparison of max-$d_{\min}$ Precoder for 16-QAM Modulation

In [41], an extension to 16-QAM modulation for optimal max-$d_{\min}$ precoder was made and exact solution was derived. Compared to QPSK case, more precoder options are selected according to the value of channel angle γ. Total of 8 different precoder expressions are calculated through the Equation (3.18), where the values of parameters for each precoder are reproduced in Table 3.3.

Because 4 bits of information are transmitted at each subcarrier for 16-QAM modulation, there are two modulation options for MRC pairing scheme which yield same spectral efficiency: i) 64-QAM modulation with $N_{\text{eff}} = \frac{2}{3}N_{\text{tot}}$ (6 bits $\times$ $\frac{2}{3}$ = 4 bits), and ii) 256-QAM modulation with $N_{\text{eff}} = \frac{1}{2}N_{\text{tot}}$ (8 bits $\times$ $\frac{1}{2}$ = 4 bits).

Figures 3.8 and 3.9 are the coded BER and average throughput performances respectively for 16-QAM modulation with the precoding schemes. As in the case for QPSK modulation, the precoding scheme II with 16-QAM modulation always outperforms the MRC pairing with higher modulation scheme in terms of both BER and throughput. But there is some point at which the MRC pairing scheme achieves better BER performance than the precoding scheme I as PLC noise density lowers. It is also noticed that the BER performance of MRC pairing with 64-QAM modulation is poorer than that of MRC pairing with 256-QAM modulation. This is due to the fact that, for 64-QAM modulation only half of effective data subcarriers are combined with remaining subcarriers for diversity ($N_{\text{eff}} = \frac{2}{3}N_{\text{tot}}$, $N_{\text{MRC}} = \frac{1}{3}N_{\text{tot}}$), while for 256-QAM modulation all effective data subcarriers are combined for diversity ($N_{\text{eff}} = N_{\text{MRC}} = \frac{1}{2}N_{\text{tot}}$).

Table 3.3: Angle values for $d_{\min}$ precoder for 16-QAM modulation [41]

Precoder	ψ (in degrees)	ϕ (in degrees)	θ (in degrees)	γ (in degrees)
F_{r1}	0	7.37	14.39	$\gamma_0 \approx 5.128$
F_{T1}	$\psi_1 = \arctan\frac{5\sqrt{2}-7}{\tan\gamma}$	45	45	$\gamma_1 \approx 5.96$
F_{T2}	45	$\phi_2 = \arcsin\frac{1}{2\cos 2\gamma}$	45	$\gamma_2 \approx 6.81$
F_{T3}	$\psi_3 = \arccos\frac{\alpha^a-\alpha\cos^2\gamma}{\alpha-2\cos^2\gamma}$	$\phi_3 = \arctan\frac{3}{5}$	45	$\gamma_3 \approx 9.45$
F_{T4}	45	$\phi_4 = \arctan\frac{\cos^2 2\gamma+1-\sqrt{6\cos^2 2\gamma-3}}{2-\cos^2 2\gamma}$	$\theta_4 = \frac{1}{2}\arctan\frac{1}{\cos\phi_4-\sin\phi_4}$	$\gamma_4 \approx 10.35$
F_{T5}	$\psi_5 = \arctan\frac{\sqrt{10/\sqrt{14}-1}}{\sqrt{10/\sqrt{14}+1}} \times \tan\gamma$	$\phi_5 = \arctan\frac{1}{3}$	$\theta_5 = \frac{1}{2}\arctan\frac{\sqrt{10}}{2}$	$\gamma_5 \approx 17.53$
F_{T6}	45	$\phi_6 = \arcsin\frac{1}{2\cos 2\gamma}$	45	$\gamma_6 \approx 22.50$
F_{T7}	$\psi_7 = \arctan\frac{\sqrt{2}-1}{\tan\gamma}$	45	45	

[a] $\alpha = 1+\frac{6}{\sqrt{34}}$

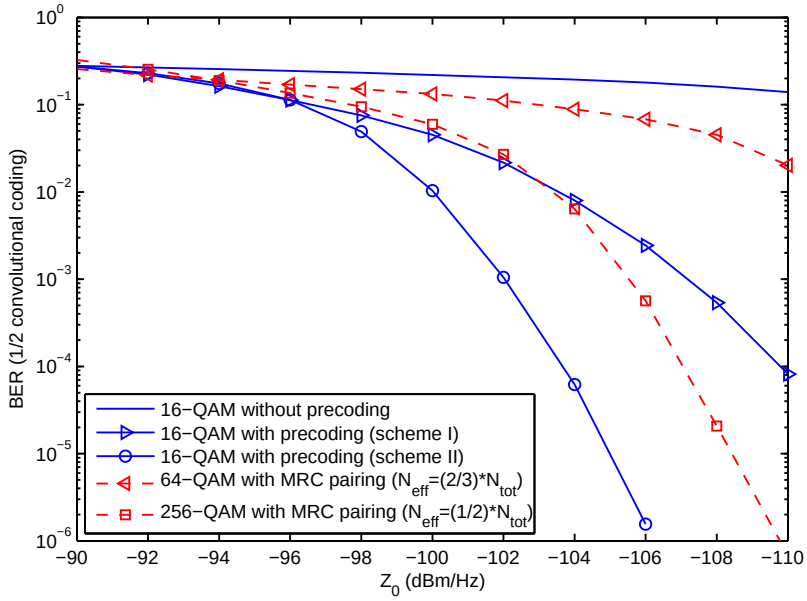

(a)

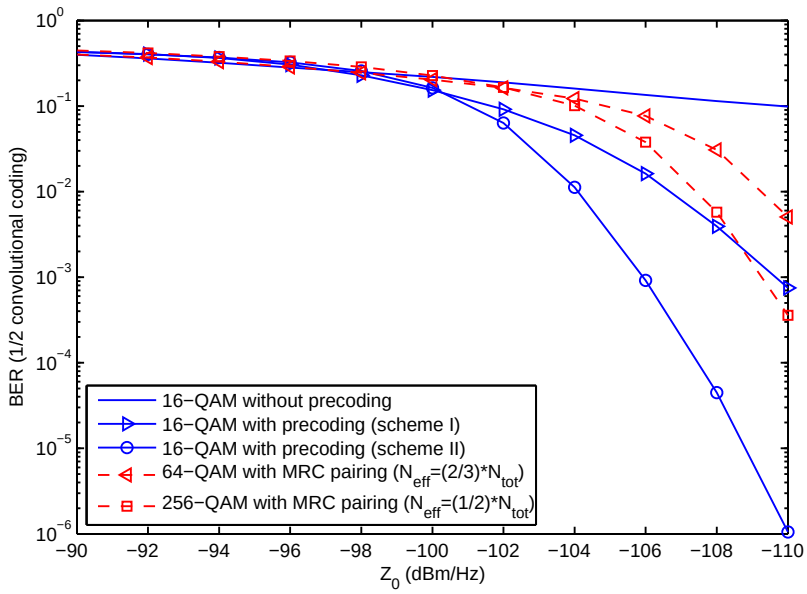

(b)

Figure 3.8: Bit error rate (BER) performance of precoding scheme for 16-QAM modulation with 1/2 convolutional coding in (a) typical urban MV topology and (b) typical rural MV topology.

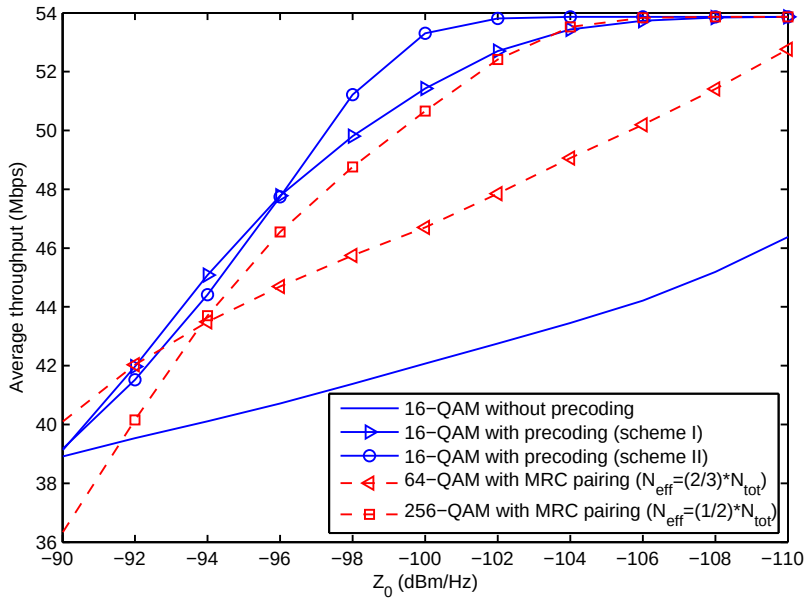

(a)

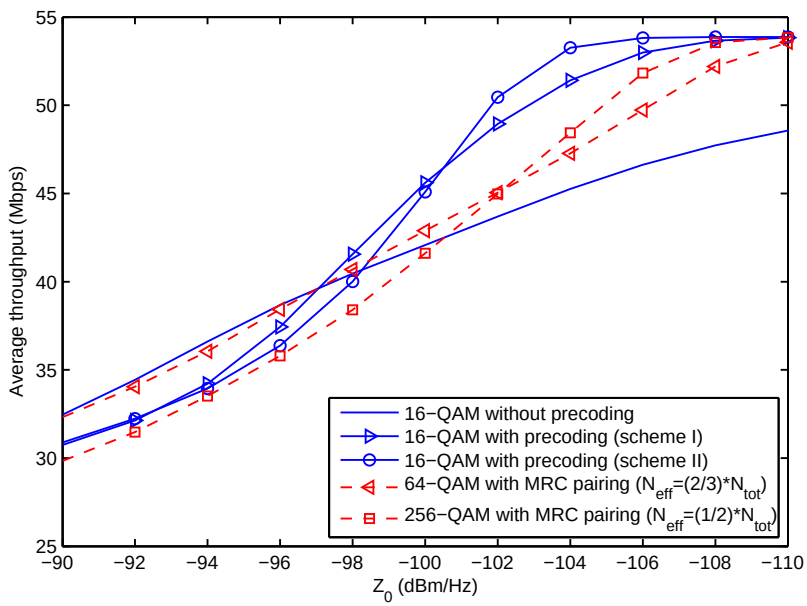

(b)

Figure 3.9: Average throughput performance of precoding scheme for 16-QAM modulation in (a) typical urban MV topology and (b) typical rural MV topology.

3.4.6 Complexity Analysis

Previous simulation results showed that the precoding scheme based on sorted SNR outperforms the proposed MRC diversity pairing scheme with higher modulation order. Both two schemes require the process of subcarrier sorting and subcarrier pairing. First we compare the detection complexity of the two schemes at the receiver. If b bits are transmitted per symbol, the modulation order M is $M = 2^b$. With the precoding scheme, two symbols are grouped and transmitted, so the search space of the ML detector is M^2. For same spectral efficiency for diversity pairing scheme, $b' = 2b$ bits per symbol should be transmitted, so in this case the modulation order $M' = 2^{2b} = M^2$. Therefore, the receiver complexity is the same for the two schemes. However, the precoding scheme requires the computation for performing virtual transformation and determining precoder at the transmitter. As described in [38], the virtual transformation requires one eigenvalue decomposition (EVD), one negative fractional power of the matrix, 6 matrix multiplications, and one singular value decomposition (SVD) for each 2×2 matrix. Figure 3.10 is the relative computation time in MATLAB for determining one precoder where the time to compute matrix multiplication is set to the reference. As shown in the figure, the computation time for performing virtual transformation is larger for calculating actual precoder. The precoding scheme requires much more computational complexity, so it is better to use the proposed MRC diversity pairing scheme with higher modulation.

3.5 Conclusion

To improve the reliability of the OFDM PLC networks, the well-known MRC concept was adopted and an optimal subcarrier pairing scheme was proposed. By combining the subcarriers for MRC with the primary data-carrying subcarriers intelligently, the performance enhancement in terms of SER was verified by numerical results. With-

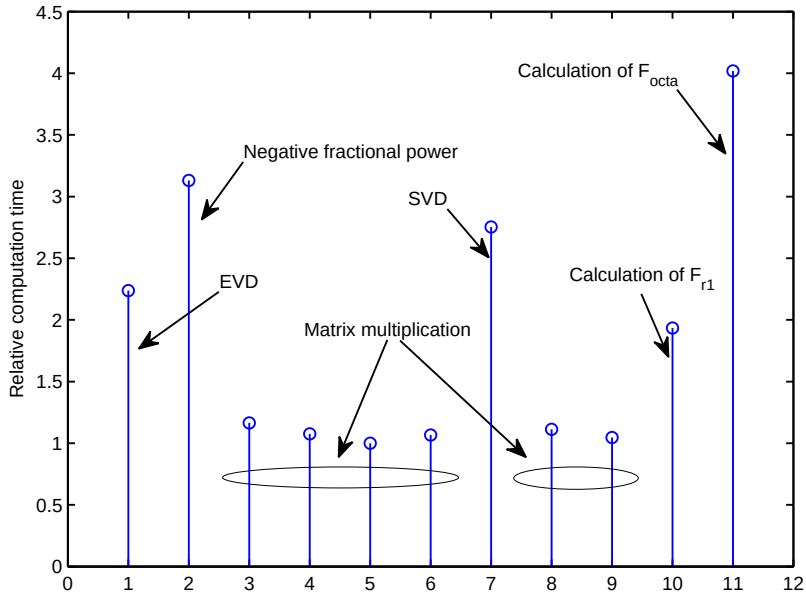

Figure 3.10: Computational overhead for determining precoder.

out much complicated matrix computation, the proposed scheme achieved comparable performance to the precoding scheme. It can also be applied to any OFDM system, especially a system with slowly varying channel characteristics.

Chapter 4

Optimal Subcarrier Pairing for MRC in Powerline/Wireless Diversity OFDM Systems

4.1 Motivation

Various communication options are available to support smart grid, as discussed in Chapter 1. The parallel use of different communication networks is expected to play a significant role in the realization of a robust smart grid communication, because the probability of different communication links simultaneously shutting down is extremely low.

As described in [43, 44, 45, 46], the powerline communication network collaborates with the wireless network, which enhances the robustness and link quality even though the powerline/wireless collaboration requires additional installation cost. A wireless relaying system assisted by the powerline network in an indoor environment has been studied in [43]. In [44], it has been proven that by combining the powerline and wireless networks, the physical layer performance can be improved and the resulting spatial diversity gain can increase the whole system throughput. It is described in [45] that a wireless/powerline combined network outperforms a single wireless or

powerline network, in smart home networking, in terms of the network energy cost, network overhead, and average latency. Furthermore, it is described in [46] that the hybrid powerline/wireless architecture forms a reliable, high-capacity, and cost-effective access network, and so has been installed in rural environments to provide both broadband services and smart grid services.

Let us consider the parallel use of powerline/wireless orthogonal frequency division multiplexing (OFDM) networks [44]. Since multiplexing approach to increase the data rate in two distinct powerline and wireless channels is relatively simple as noted in [44], it is assumed that a data symbol is simultaneously transmitted through both the powerline and wireless subcarriers to enhance reliability by using the powerline/wireless diversity combining. The receiver is assumed to perform maximal ratio combining (MRC) or saturated metric combining (SMC), which are considered to be practical schemes. It can be noted that, in [44], an OFDM signal is generated by a single OFDM modulator and two identical copies of the OFDM signal are transmitted via both the powerline and wireless channels. This implies that the powerline and wireless networks should use the same OFDM parameters.

The powerline and wireless OFDM systems considered in this study have different numbers of subcarriers. Further, two independent OFDM modulators are used so different OFDM signals are transmitted via the powerline and wireless channels. Since SMC requires additional parameters to characterize the impulsive noise in powerline channels and is specialized for maximum-likelihood (ML) detection [44], we focus on MRC and propose an optimal subcarrier pairing scheme for MRC in powerline/wireless diversity OFDM systems to determine the wireless subcarrier that should be paired with a given powerline subcarrier to transmit the same data symbol.

The rest of this chapter is organized as follows. Section 4.2 describes powerline/wireless diversity channels and analyzes the information theoretic performance. In Section 4.3, we propose an optimal subcarrier pairing scheme to maximize the data

rate for MRC diversity reception. Numerical results are presented in Section 4.4 to verify the performance enhancement of the proposed scheme. Finally, conclusions are drawn in Section 4.5. The notations used in this chapter are listed in Table 4.1.

4.2 Powerline/Wireless Diversity OFDM Systems

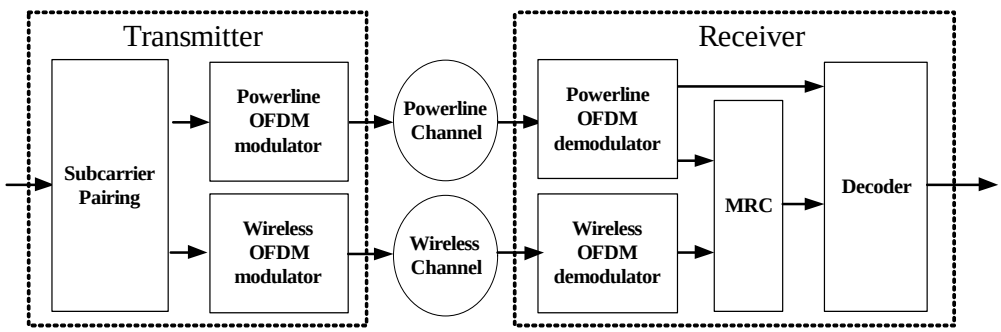

Figure 4.1: Block diagram of powerline/wireless diversity OFDM system.

Let us consider a powerline/wireless diversity OFDM system as shown in Figure 4.1. As described in [46], a wireless network operates alternatively as or cooperatively with a powerline network. In this study, we assume that the objective of the wireless network is to cooperate with the powerline network, and thereby the wireless network assists the powerline network. All the powerline subcarriers are assumed to carry different data symbols, and one of the wireless subcarriers is paired with a powerline subcarrier. The paired powerline and wireless subcarriers are modulated using the same data symbol and thereby the wireless connection achieves network survivability in the case where the powerline connection is lost [46]. The number of subcarriers for the powerline and wireless OFDM systems are denoted as N^{P} and N^{W}, respectively. In this study, we consider two different scenarios as follows:

- When $N^{\mathrm{P}} > N^{\mathrm{W}}$, N^{W} powerline subcarriers among N^{P} subcarriers are paired with N^{W} wireless subcarriers and $N^{\mathrm{P}} - N^{\mathrm{W}}$ powerline subcarriers are used with-

Table 4.1: Summary of the notations used in Chapter 4

Notation	Definition
N^{P}	The number of subcarriers of the powerline system
N^{W}	The number of subcarriers of the wireless system
Γ	The set of the indices of the powerline subcarriers to be paired with the wireless subcarriers
p_i	Subcarrier index of powerline system
q_i	Subcarrier index of wireless system which is paired with p_ith subcarrier
χ_i	Subcarrier pairing for p_ith powerline subcarrier. For $p_i \in \Gamma$, $\chi_i = (p_i, q_i)$ and for $p_i \notin \Gamma$, $\chi_i = p_i$
$y^P[p_i]$	Received signal by the powerline system at the p_ith subcarrier
$H^P[p_i]$	Powerline complex channel coefficient at the p_ith subcarrier
$s[p_i]$	Data symbol transmitted at the p_ith subcarrier
P^P	Transmit power of the powerline system at each subcarrier
$z^P[p_i]$	Colored background noise of the powerline at the p_ith subcarrier
$Z^P[p_i]$	Variance of the $z^P[p_i]$
$y^W[q_i]$	Received signal by the wireless system at the q_ith subcarrier
$H^W[q_i]$	Wireless complex channel coefficient at the q_ith subcarrier
P^W	Transmit power of the wireless system at each subcarrier
$z^W[q_i]$	AWGN of the wireless system at the q_ith subcarrier with a variance of Z^W
$\gamma^P[p_i]$	SNR of the powerline system at the p_ith subcarrier
$\gamma^W[q_i]$	SNR of the wireless system at the q_ith subcarrier
$y_{\mathrm{MRC}}[\chi_i]$	Received signal after the MRC over the subcarrier pair χ_i
$z_{\mathrm{MRC}}[\chi_i]$	Additive noise after the MRC over the subcarrier pair χ_i
$\gamma_{\mathrm{MRC}}[\chi_i]$	SNR after the combining through the subcarrier pair χ_i

out pairing.

- When $N^{\mathrm{P}} \leq N^{\mathrm{W}}$, N^{P} wireless subcarriers among N^{W} subcarriers assist N^{P} powerline subcarriers and the remaining $N^{\mathrm{W}} - N^{\mathrm{P}}$ wireless subcarriers are assumed to be used for other wireless services.

Let us define Γ as a set of indices of the powerline subcarriers to be paired with the wireless subcarriers with a cardinality of $|\Gamma| \leq N^{\mathrm{P}}$.

The signal received by the powerline receiver at the p_ith subcarrier can be expressed as

$$y^{\mathrm{P}}[p_i] = H^{\mathrm{P}}[p_i]\sqrt{P^{\mathrm{P}}}s[p_i] + z^{\mathrm{P}}[p_i], \tag{4.1}$$

where $s[p_i]$ denotes the data symbol transmitted at the p_ith subcarrier with $\mathcal{E}\left\{|s[p_i]|^2\right\} = 1$, $H^{\mathrm{P}}[p_i]$ is the powerline complex channel coefficient at the p_ith subcarrier, P^{P} denotes the transmit power of the powerline transmitter at each subcarrier, and $z^{\mathrm{P}}[p_i]$ is the colored background noise at the powerline receiver with a variance of $Z^{\mathrm{P}}[p_i]$. For $p_i \in \Gamma$, we assume the subcarrier pairing of $\chi_i = (p_i, q_i)$, where both the p_ith powerline subcarrier and the q_ith wireless subcarrier carry the same data symbol. For $p_i \notin \Gamma$, the subcarrier pairing is simply expressed as $\chi_i = p_i$. The signal received by the wireless receiver at the q_ith subcarrier is expressed as

$$y^{\mathrm{W}}[q_i] = H^{\mathrm{W}}[q_i]\sqrt{P^{\mathrm{W}}}s[p_i] + z^{\mathrm{W}}[q_i], \tag{4.2}$$

where $H^{\mathrm{W}}[q_i]$ is the wireless complex channel coefficient, P^{W} denotes the transmit power of the wireless transmitter at each subcarrier, and $z^{\mathrm{W}}[q_i]$ is the additive white Gaussian noise (AWGN) at the wireless receiver with a variance of Z^{W}.

For $p_i \in \Gamma$, the received signals in (4.1) and (4.2) are combined using the MRC [44] expressed as

$$\begin{aligned} y_{\mathrm{MRC}}[\chi_i] &= \frac{\sqrt{P^{\mathrm{P}}}\left(H^{\mathrm{P}}[p_i]\right)^*}{Z^{\mathrm{P}}[p_i]} y^{\mathrm{P}}[p_i] + \frac{\sqrt{P^{\mathrm{W}}}\left(H^{\mathrm{W}}[q_i]\right)^*}{Z^{\mathrm{W}}} y^{\mathrm{W}}[q_i] \\ &= \left(\frac{\left|H^{\mathrm{P}}[p_i]\right|^2 P^{\mathrm{P}}}{Z^{\mathrm{P}}[p_i]} + \frac{\left|H^{\mathrm{W}}[q_i]\right|^2 P^{\mathrm{W}}}{Z^{\mathrm{W}}} \right) s[p_i] + z_{\mathrm{MRC}}[\chi_i], \end{aligned} \tag{4.3}$$

where

$$y_{\mathrm{MRC}}[\chi_i] = \frac{\sqrt{P^{\mathrm{P}}}(H^{\mathrm{P}}[p_i])^*}{Z^{\mathrm{P}}[p_i]} z^{\mathrm{P}}[p_i] + \frac{\sqrt{P^{\mathrm{W}}}(H^{\mathrm{W}}[q_i])^*}{Z^{\mathrm{W}}} z^{\mathrm{W}}[q_i]. \tag{4.4}$$

When $N^{\mathrm{P}} \leq N^{\mathrm{W}}$, $p_i \in \Gamma$ for all i. When $N^{\mathrm{P}} > N^{\mathrm{W}}$, however, there exists $p_i \notin \Gamma$ and the received signal in (4.1) is demodulated without combining. The instantaneous signal-to-noise ratio (SNR) at the p_ith subcarrier can be given as

$$\gamma^{\mathrm{MRC}}[\chi_i] = \begin{cases} \gamma^{\mathrm{P}}[p_i] + \gamma^{\mathrm{W}}[q_i], & p_i \in \Gamma \quad (4.5) \\ \gamma^{\mathrm{P}}[p_i], & p_i \notin \Gamma, \quad (4.6) \end{cases}$$

where $\gamma^{\mathrm{P}}[p_i] = \frac{\left|H^{\mathrm{P}}[p_i]\right|^2 P^{\mathrm{P}}}{Z^{\mathrm{P}}[p_i]}$ and $\gamma^{\mathrm{W}}[q_i] = \frac{\left|H^{\mathrm{W}}[q_i]\right|^2 P^{\mathrm{W}}}{Z^{\mathrm{W}}}$. For a given set of subcarrier pairings $\chi = \{\chi_1, \chi_2, \cdots, \chi_{N^{\mathrm{P}}}\}$, the whole data rate is computed [47] as

$$\mathrm{R}(\chi) = \sum_{i=1}^{N^{\mathrm{P}}} \log_2 \left(1 + \gamma^{\mathrm{MRC}}[\chi_i]\right) \Delta f, \tag{4.7}$$

where Δf denotes the subcarrier spacing. It can be noted that the MRC in (4.3) can be used even in the case where the powerline and wireless systems comprise different OFDM parameters. However, we assume that the subcarrier spacing is the same for the sake of analytical simplicity in (4.7).

4.3 Optimal Subcarrier Pairing for Powerline/Wireless Diversity

In this section, we discuss on the determination of the subcarrier pairings χ for maximizing (4.7), which is expressed as

$$\chi^{opt} = \arg\max_{\chi} \ \mathrm{R}(\chi). \tag{4.8}$$

For a simple pairing, we can set $p_i = q_i = i$ with $p_i \in \Gamma$ and the other subcarrier with $p_i \notin \Gamma$ is used without pairing. When $N^{\mathrm{P}} = N^{\mathrm{W}}$ and a simple pairing is employed, the

powerline/wireless OFDM system in Figure 4.1 is identical to that in [44]. Therefore, it is obvious that the case considered in [44] is a special case of the powerline/wireless OFDM system shown in Figure 4.1. In this study, let us assume that the channel quality of each of the subcarriers is fed back to the transmitter. Further, we can derive the optimal subcarrier pairing χ^{opt}.

In (4.5) and (4.6), ρ_i is defined as the ith smallest value among $\gamma^{\mathrm{P}}[i]$ with $i = 1,2,\cdots,N^{\mathrm{P}}$, and the corresponding subcarrier index is denoted as α_i. Similarly, τ_i is defined as the ith largest value among $\gamma^{\mathrm{W}}[i]$ with $i = 1,2,\cdots,N^{\mathrm{W}}$ and the corresponding subcarrier index is denoted as β_i. Further, we consider $0 < \rho_1 < \rho_2 < \cdots < \rho_{N^{\mathrm{P}}}$ and $\tau_1 > \tau_2 > \cdots > \tau_{N^{\mathrm{W}}} > 0$.

First, we consider that one of the two powerline subcarriers with the SNRs of ρ_i and ρ_j is paired with the wireless subcarrier with an SNR of τ_k and the other one is used without pairing. Let us reexamine the inequality (3.7) in previous chapter. If we assume that $a_1 = \rho_i$, $a_2 = \rho_j$, $\Delta_1 = 1$, and $\Delta_2 = 1+\tau_k$, (3.7) leads to for $\rho_i < \rho_j$

$$\begin{aligned}\log_2(1+\rho_i+\tau_k)+\log_2(1+\rho_j)\\ -\log_2(1+\rho_j+\tau_k)-\log_2(1+\rho_i)>0.\end{aligned} \tag{4.9}$$

This implies that the powerline subcarrier with a higher SNR should be used without pairing. As a result, the powerline subcarrier indices are sorted in ascending order of their SNRs and let Γ include the first N^{W} of the sorted subcarrier indices.

Now, let us consider the pairing between the powerline subcarriers in Γ and N^{W} wireless subcarriers. When $\rho_i < \rho_j$ and $\tau_k > \tau_l$, it is observed that the following inequality holds from (3.7) with $a_1 = \rho_i$, $a_2 = \rho_j$, $\Delta_1 = 1+\tau_l$, and $\Delta_2 = 1+\tau_k$:

$$\begin{aligned}\log_2(1+\rho_i+\tau_k)+\log_2(1+\rho_j+\tau_l)\\ -\log_2(1+\rho_i+\tau_l)-\log_2(1+\rho_j+\tau_k)>0.\end{aligned} \tag{4.10}$$

It is observed in (4.10) that the powerline subcarrier with a lower SNR should be paired with the wireless subcarrier with a higher SNR to increase the data rate. Therefore,

we conclude that the wireless subcarrier indices are sorted in descending order of their SNRs and sequentially paired with the powerline subcarrier indices sorted in ascending order of their SNRs.

With the above observation, we summarize the optimal subcarrier pairing scheme as follows.

- The powerline subcarriers are sorted in ascending order of their SNRs, which yields the sorted subcarrier indices $\{\alpha_1, \alpha_2, \cdots, \alpha_{N^{\mathrm{P}}}\}$
- When $N^{\mathrm{P}} > N^{\mathrm{W}}$, N^{W} wireless subcarriers are sorted in descending order of their SNRs. The sorted subcarrier indices are expressed as $\{\beta_1, \beta_2, \cdots, \beta_{N^{\mathrm{W}}}\}$ and $\Gamma = \{\alpha_1, \alpha_2, \cdots, \alpha_{N^{\mathrm{W}}}\}$.
- When $N^{\mathrm{P}} \leq N^{\mathrm{W}}$, N^{P} wireless subcarriers with the highest SNRs are selected among N^{W} wireless subcarriers. The selected subcarriers are sorted in a descending order of their SNRs. The sorted subcarrier indices are given as $\{\beta_1, \beta_2, \cdots, \beta_{N^{\mathrm{P}}}\}$ and $\Gamma = \{\alpha_1, \alpha_2, \cdots, \alpha_{N^{\mathrm{P}}}\}$.
- For $\alpha_i \in \Gamma$, the subcarrier pairing is performed as $\chi_i^{opt} = (\alpha_i, \beta_i)$. For $\alpha_i \notin \Gamma$, the powerline subcarrier is used without pairing and $\chi_i^{opt} = \alpha_i$.

4.4 Numerical Results

In this section, we present the evaluation results of the ergodic data rate and outage probability of the proposed subcarrier pairing scheme using the Monte Carlo simulation. The performance of the simple pairing scheme described in Section 4.3 is evaluated for the sake of comparison. The powerline OFDM system comprises $N^{\mathrm{P}} = 1536$ subcarriers with a 30 MHz bandwidth and the useful OFDM symbol duration is 51.2 μs [33]. The transmit power of the powerline transmitter is assumed to be -60 dBm/Hz [20]. The wireless OFDM system is set to comprise the same subcarrier spacing with $N^{\mathrm{W}} = 1024$ or 2048 occupying a 20 MHz and 40 MHz bandwidth,

respectively. For same transmit power per subcarrier, the total transmit power of the wireless system is set to be 40 dBm and 43 dBm [48] for each value of N^{W}. OFDM parameters for simulation are summarized in Table 4.2.

Table 4.2: OFDM parameters for simulation in Chapter 4

	PLC	Wireless Systems	
		$N^{\mathrm{W}} = 1024$	$N^{\mathrm{W}} = 2048$
Parameter	Value		
FFT size	2048		
Sampling clock	40 [MHz]		
OFDM subcarrier spacing, Δf	19.5312 [kHz]		
useful OFDM symbol duration, $1/\Delta f$	51.2 [μs]		
Total number of subcarriers	1536	1024	2048
Occupied bandwidth	30 [MHz]	20 [MHz]	40 [MHz]

4.4.1 Channel Models

While we only considered the colored background noise for PLC channel in previous chapter, the impulsive noise, which makes the channel environment more harsh, are added in this study. The added impulsive noise is represented by

$$\frac{\sigma}{m} Z_1^{\mathrm{P}}. \tag{4.11}$$

As depicted in Figure 4.2, FFT in OFDM receiver spreads impulsive energy over all tones, so the impulsive noise causes the SNR in each subcarrier to decrease. We assume that σ impulsive noises occur in one useful OFDM symbol duration and each impulsive noise sample follows an i.i.d. complex Gaussian with zero mean and $Z_1^{\mathrm{P}} \Delta f$ variance. As described in [12], the impulse events occur at a rate of approximately 165 impulses per second (imp/sec). However, for MV powerlines, there are a few

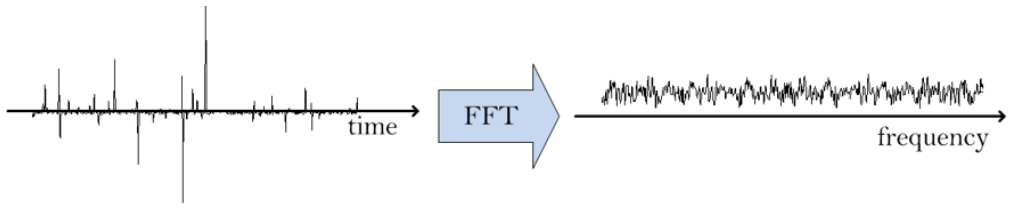

Figure 4.2: Effect of impulsive noise in frequency domain.

studies conducted to characterize the impulsive noise characteristic. In this study, we assume that σ varies between 0 and 10, which implies that the impulse rate is between 0 imp/sec, in the best case, and 195312.5 imp/sec, in the worst case. Moreover, m denotes the FFT size of the powerline OFDM and the variance of the impulsive noise Z_1^{P} is assumed to be 30 dB greater than the variance of the colored background noise Z_0^{P} [24]. Therefore, the overall power spectral density of the powerline noise can be expressed as

$$Z^{\mathrm{P}}[i] = Z_0^{\mathrm{P}} + 37\exp[-0.17\times 10^{-6}(f_L + \Delta f \cdot i)] + \frac{\sigma}{m} Z_1^{\mathrm{P}} \text{ (dBm/Hz)}. \tag{4.12}$$

We consider the typical suburban topology for PLC channel environment. Please refer to the Table 2.1 and Figure 2.6.

The wireless channel is modeled as the IEEE 802.16j channel models of type D for suburban environments [49]. We have evaluated the propagation loss in the 2 GHz band by assuming that the transmitter and receiver are located above the rooftop. It is reasonable to assume that the wireless system is mounted on the MV power grids, because the transmitter and receiver are assumed to be located on MV power grids. Figure 4.3 is the path loss of considered channel model.

The statistical parameters such as tapped delay line, fading, and antenna directivity have been used based on three-tap SUI-1 channel model [49] as summarized in Table 4.3. The magnitude of channel gain in frequency domain for several channel realizations are depicted in Figure 4.4.

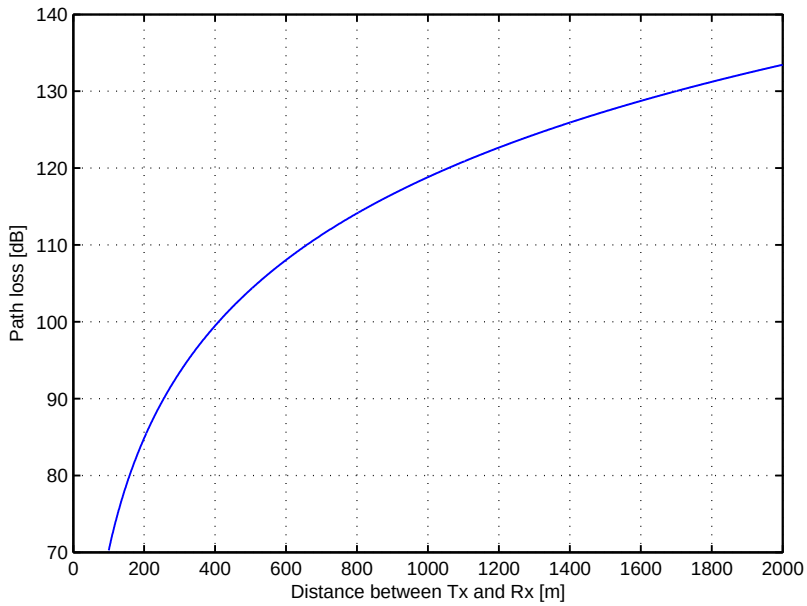

Figure 4.3: Path loss of IEEE 802.16j, type D model for 2 GHz.

Table 4.3: SUI-1 channel model parameters

	Tap 1	Tap 2	Tap 3	Unit
Delay	0	0.4	0.9	μs
Power	0	-15	-20	dB
K-factor	4	0	0	
Doppler	0.4	0.3	0.5	Hz

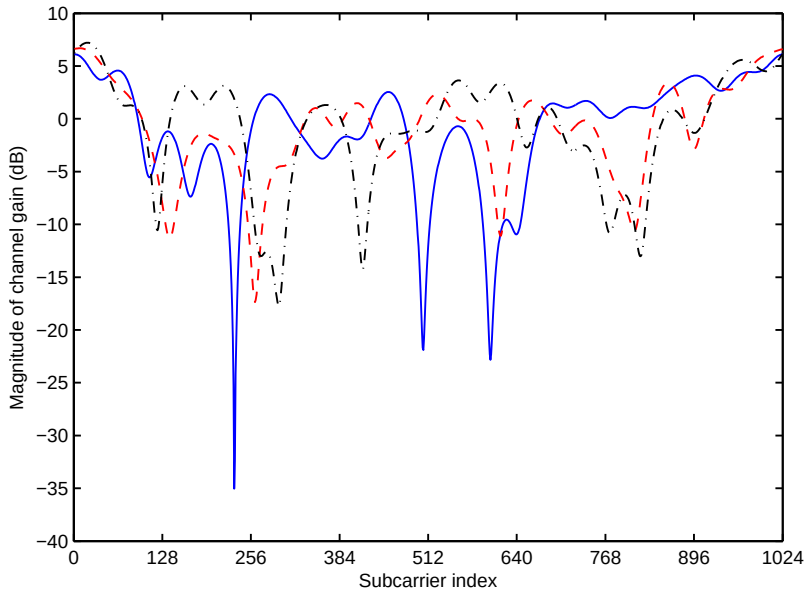

(a) $N^{\mathrm{W}} = 1024$

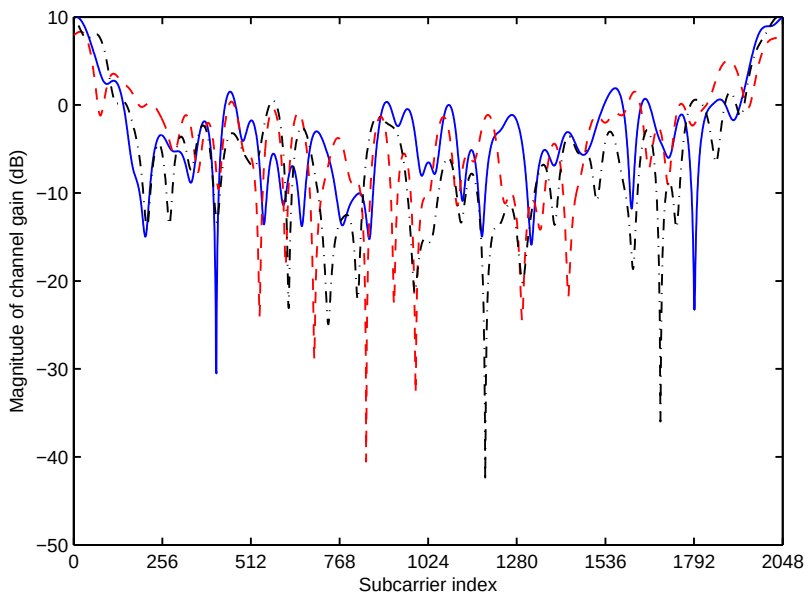

(b) $N^{\mathrm{W}} = 2048$

Figure 4.4: Example of SUI-1 wireless channel realizations.

The noise variance of the wireless system Z^{W} is calculated as $-173.8+NF$ dBm/Hz, where the receiver noise figure NF is 7 dB.

4.4.2 Performance Comparison

As mentioned in Section 4.3, the proposed optimal pairing scheme requires the channel quality feedback. The feedback information should include channel coefficient and SNR for each subcarrier. We assume that the transmitter and the receiver agree to use same pairing scheme in advance, so actual subcarrier pairing information need not be exchanged. But in practical systems, the instantaneous feedback of the channel quality of each subcarrier at each OFDM symbol is not feasible. Therefore we consider two different feedback scenarios; i) *instantaneous feedback*, where current channel realization is immediately reflected in subcarrier sorting/pairing process as well as current data transmission; ii) *outdated feedback*, where the subcarrier sorting/pairing is based on the previous channel realization.

Figure 4.5 shows the ergodic data rate achieved by the proposed optimal pairing scheme in a typical suburban environment at varying Z_0^{P} when $\sigma = 4$. Capacity gain compared to the case in which only powerline is used for transmission is depicted in Figure 4.6. To illustrate the performance improvement through the proposed pairing scheme, capacity gain over simple pairing scheme also is presented in Figure 4.7.

Through the proposed scheme with instantaneous feedback, about 15–20 Mbps for $N^{\mathrm{W}} = 1024$ and 20–30 Mbps for $N^{\mathrm{W}} = 2048$ increase of data rates are achieved compared to the simple pairing case. The proposed scheme outperforms the simple pairing even with the outdated feedback where the increase of data rates is about 10–15 Mbps. When $N^{\mathrm{W}} = 1024$ ($N^{\mathrm{P}} > N^{\mathrm{W}}$), performance degradation due to outdated feedback is small, but the degradation is more pronounced when $N^{\mathrm{W}} = 2048$ ($N^{\mathrm{P}} \leq N^{\mathrm{W}}$).

By using auxiliary wireless channel for transmission, significant capacity gain can be achieved. When the powerline channel is bad with high noise density of

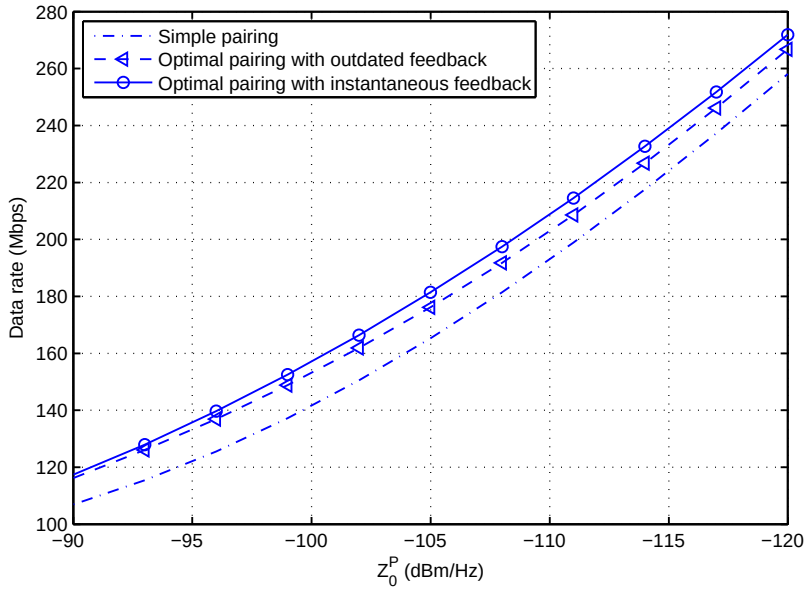

(a) $N^W = 1024$

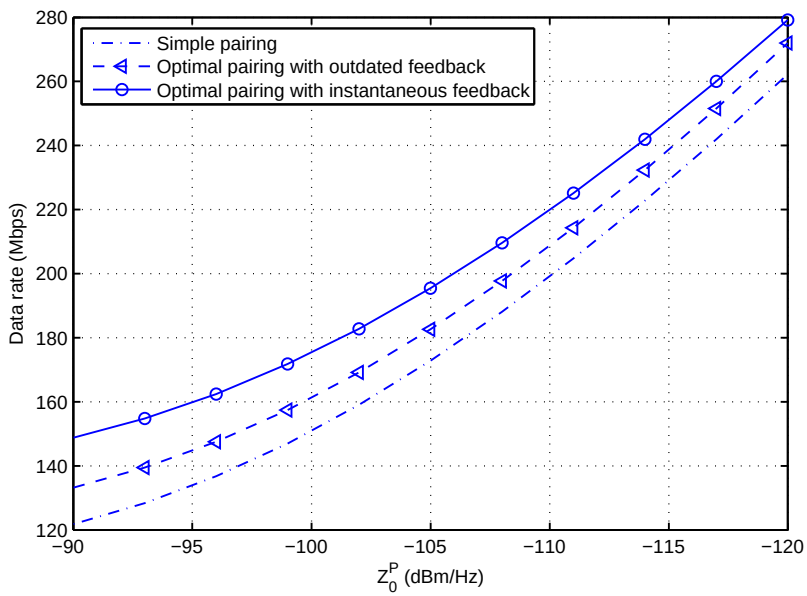

(b) $N^W = 1024$

Figure 4.5: Ergodic data rates with respect to Z_0^P when $\sigma = 4$.

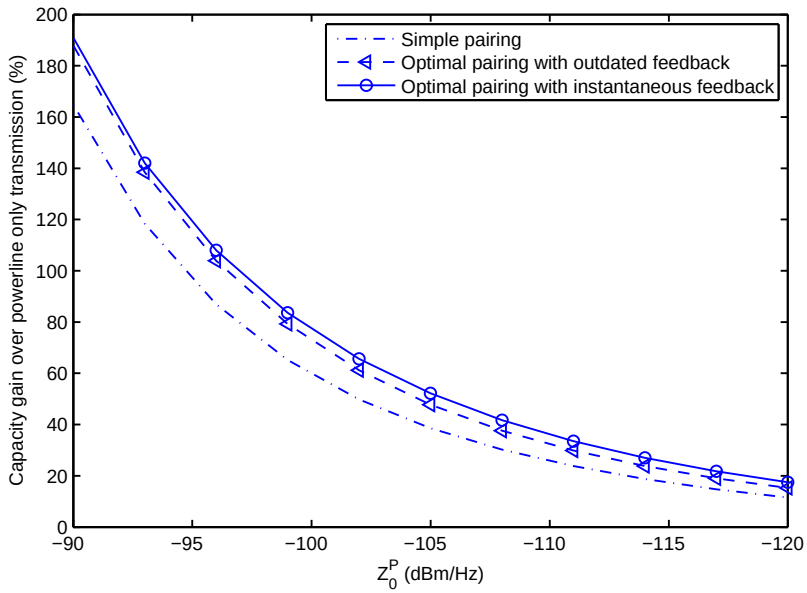

(a) $N^W = 1024$

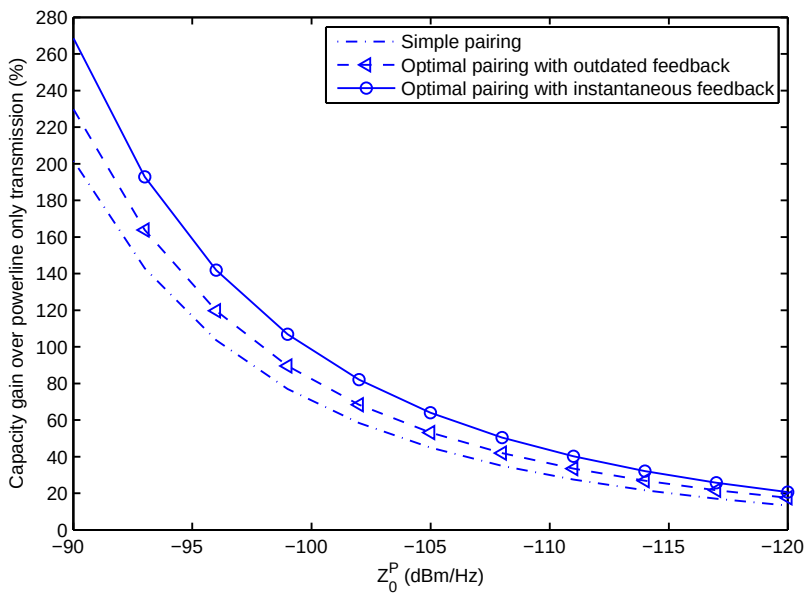

(b) $N^W = 2048$

Figure 4.6: Capacity gain over powerline only transmission with respect to Z_0^P when $\sigma = 4$.

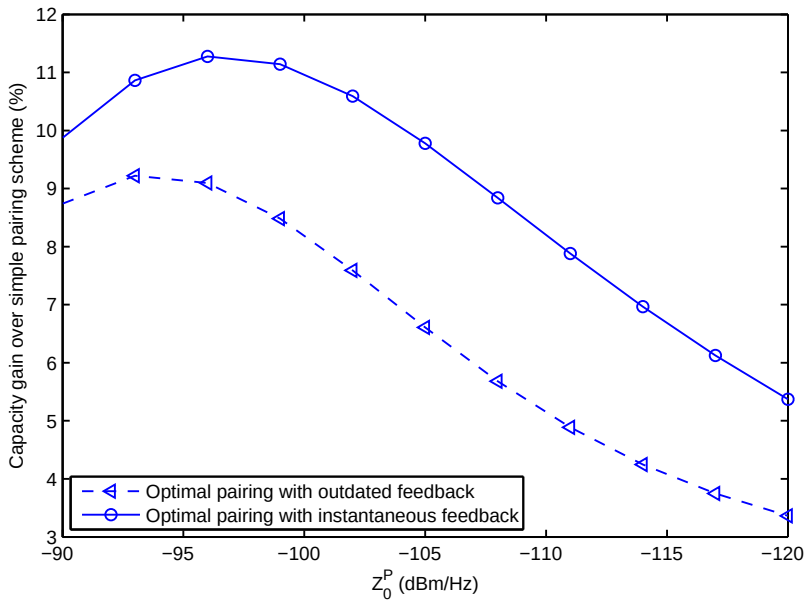

(a) $N^W = 1024$

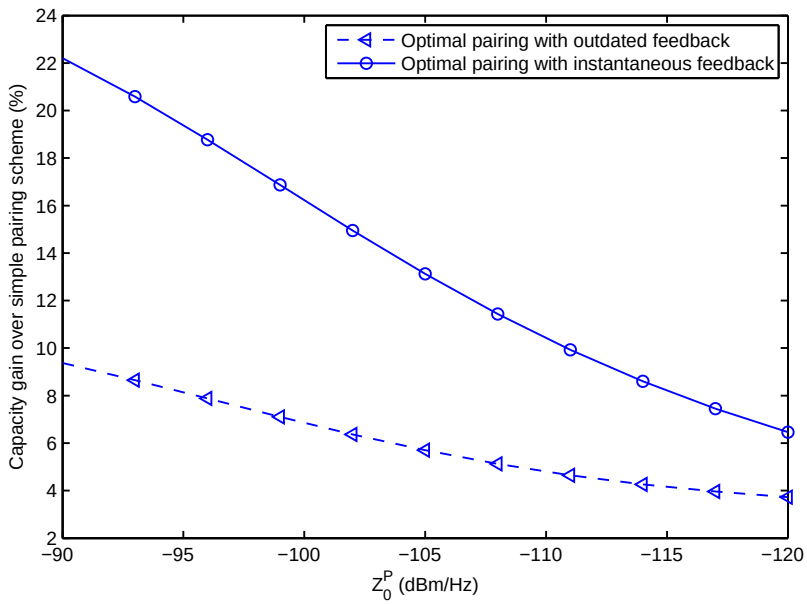

(b) $N^W = 2048$

Figure 4.7: Capacity gain over simple pairing scheme with respect to Z_0^P when $\sigma = 4$.

$Z_0^{\mathrm{P}} = -90$ dBm/Hz, almost 200 % of gain for $N^{\mathrm{W}} = 1024$ is shown in Figure 4.6. This gain comes from that the subcarriers of powerline system having very low SNRs are compensated by the subcarriers of wireless system having relatively high SNRs. As the noise density of powerline channel is lowered, the capacity gain also decreases but still about 20 % of gain is achieved when $Z_0^{\mathrm{P}} = -120$ dBm/Hz. The gain is larger for $N^{\mathrm{W}} = 2048$ compared to for $N^{\mathrm{W}} = 1024$, because more subcarriers of powerline systmes are combined with those of wireless systems.

Capacity gain due to optimal pairing scheme over simple pairing scheme is about 3–9 % for outdated feedback case, and about 5–11 % for instantaneous feedback case, when $N^{\mathrm{W}} = 1024$. With $N^{\mathrm{W}} = 2048$, much larger capacity gain about 6–22 % over simple pairing scheme is shown for instantaneous feedback case, but similar gain about 4–10 % is shown for outdated feedback case compared to when $N^{\mathrm{W}} = 1024$. While the gain difference between two feedback case is almost constant with 2–3 % when $N^{\mathrm{W}} = 1024$, the difference increases as Z_0^{P} increases when $N^{\mathrm{W}} = 2048$.

Figure 4.8 is the ergodic data rate with respect to varying impulsive noise rate parameter σ for $Z_0^{\mathrm{P}} = -100$ dBm/Hz. Corresponding capacity gain graphs are depicted in Figure 4.9 and Figure 4.10. Simulation results show that as the impulsive noise increases, the achievable data rate decreases, but the relative capacity gain increases. Performance gap between two feedback case is more outstanding for $N^{\mathrm{W}} = 2048$.

We also evaluated the outage probability of the proposed scheme. The outage probability is defined as the probability that the instantaneous rate is less than the given threshold, R_{th}. It is worth mentioning that we can use the outage probability to measure the system reliability when R_{th} is considered as a target data rate. Figure 4.11 compares the outage probabilities of the simple pairing and the proposed optimal pairing schemes when $Z_0^{\mathrm{P}} = -100$ dBm/Hz and $\sigma = 4$. It is observed that the proposed scheme provides enhanced outage performance. When $N^{\mathrm{W}} = 1024$ and $R_{th} = 144$ Mbps, the outage probabilities of the simple pairing scheme and the proposed scheme with out-

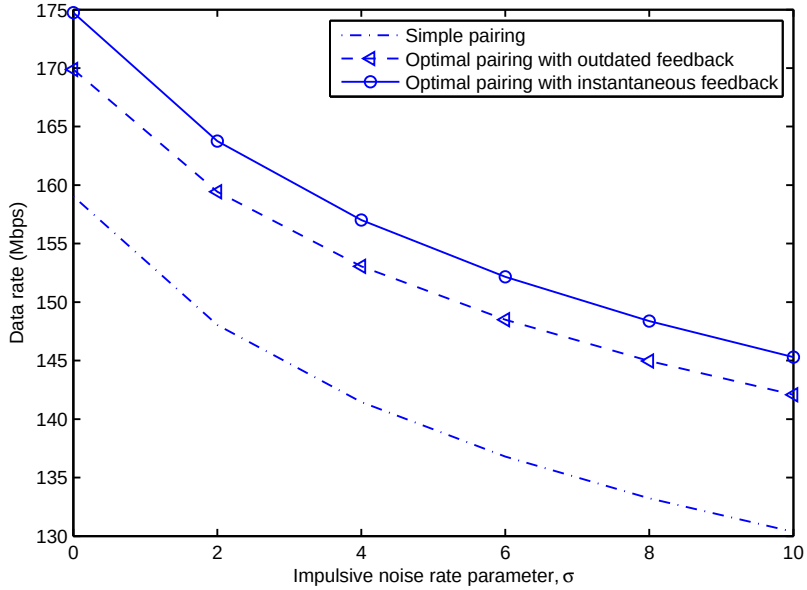

(a) $N^{\mathrm{W}} = 1024$

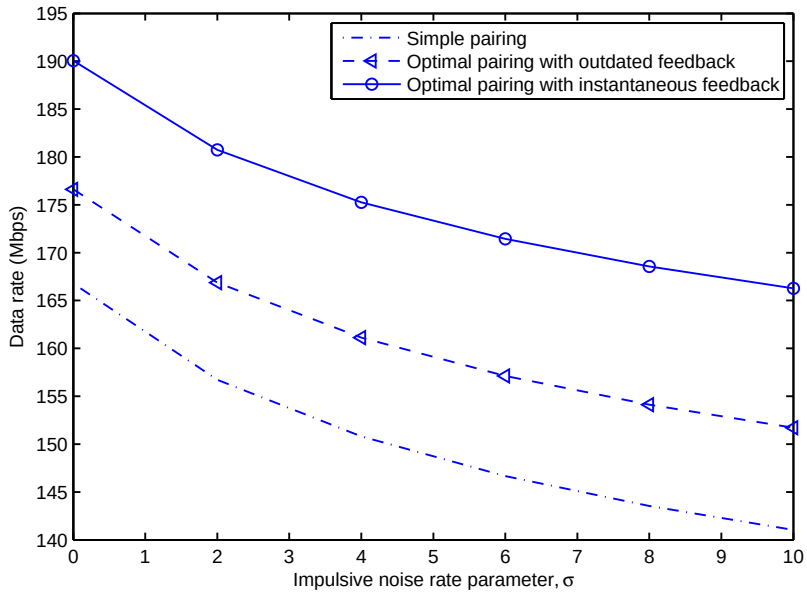

(b) $N^{\mathrm{W}} = 2048$

Figure 4.8: Ergodic data rates with respect to σ when $Z_0^{\mathrm{P}} = -100$ dBm/Hz.

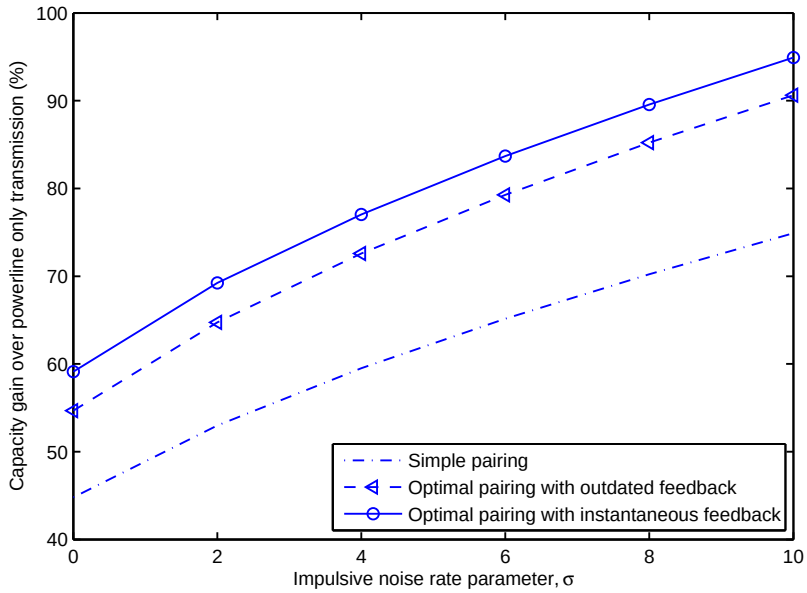

(a) $N^{\mathrm{W}} = 1024$

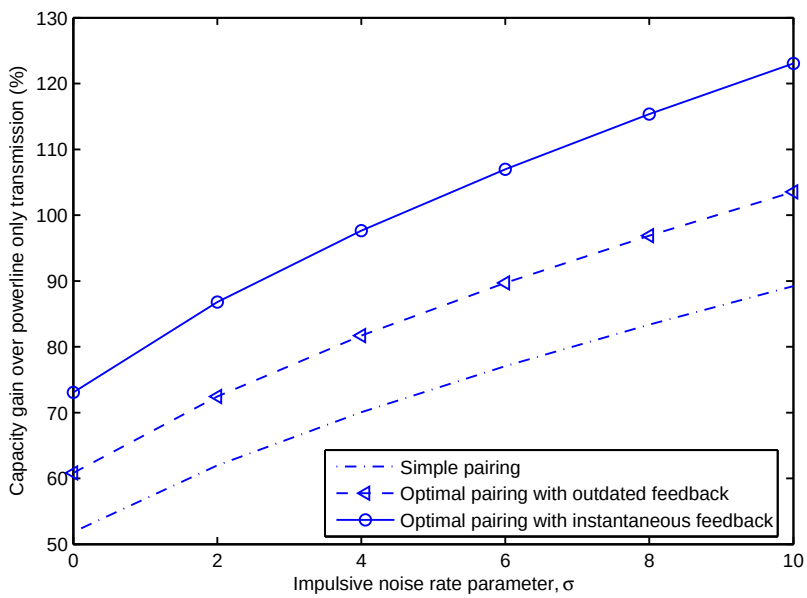

(b) $N^{\mathrm{W}} = 2048$

Figure 4.9: Capacity gain over powerline only transmission with respect to σ when $Z_0^{\mathrm{P}} = -100$ dBm/Hz.

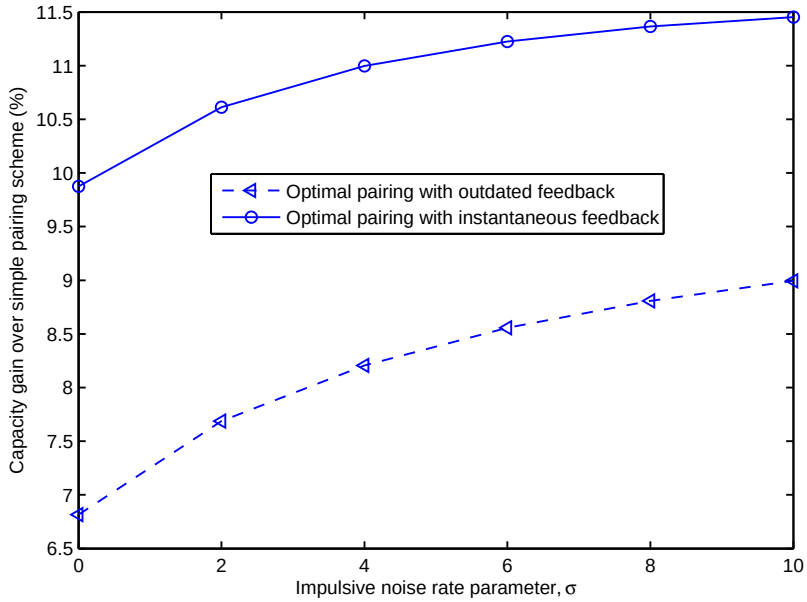

(a) $N^{\mathrm{W}} = 1024$

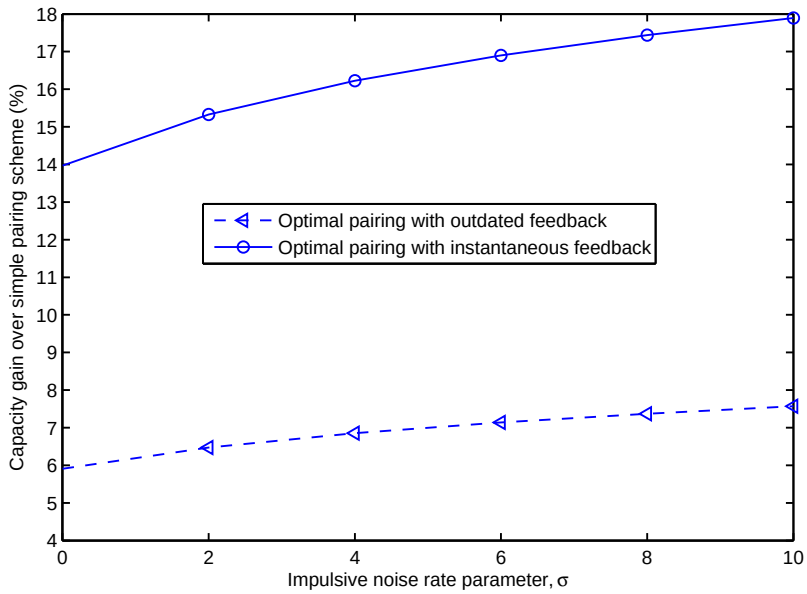

(b) $N^{\mathrm{W}} = 2048$

Figure 4.10: Capacity gain over simple pairing scheme with respect to σ when $Z_0^{\mathrm{P}} = -100$ dBm/Hz.

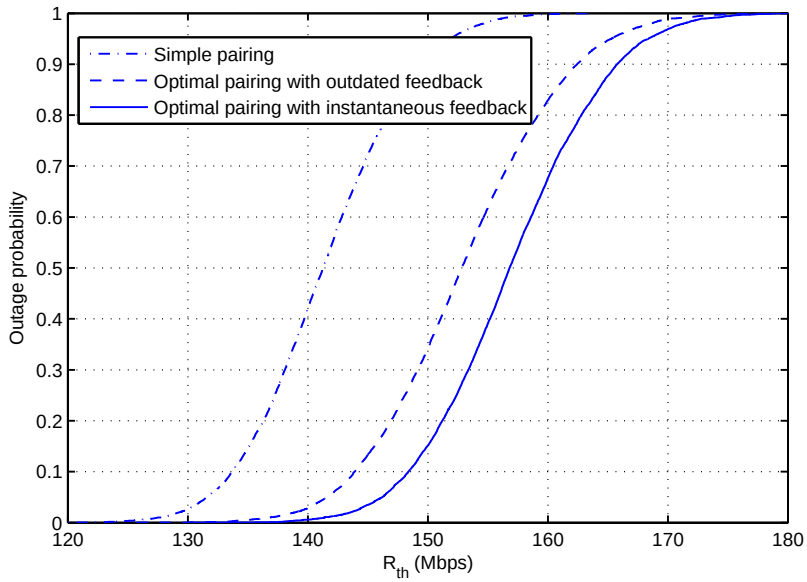

(a) $N^{\mathrm{W}} = 1024$

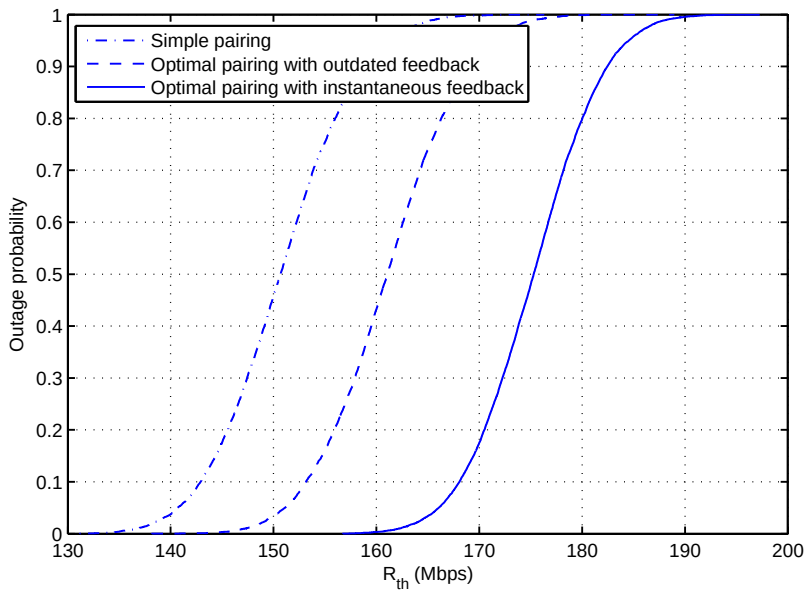

(b) $N^{\mathrm{W}} = 2048$

Figure 4.11: Outage probability with respect to target data rate R_{th} when $Z_0^{\mathrm{P}} = -100$ dBm/Hz and $\sigma = 4$.

dated feedback are found to be about 0.67 and 0.10, respectively. This implies that the simple pairing scheme cannot achieve the target data rate of $R_{th} = 144$ Mbps with the probability of 67%, whereas the probability that the proposed scheme fails to achieve $R_{th} = 144$ Mbps is only 10%. Regardless of the number of subcarriers of wireless system, the difference between the target data rate which produces same outage probability for simple pairing and optimal pairing with outdated feedback cases is almost same with 10 Mbps. On the contrary, the difference between the target data rate which produces same outage probability for two feedback cases is much larger when $N^{\mathrm{W}} = 2048$.

4.5 Conclusion

In this chapter, we have proposed an optimal subcarrier pairing scheme for powerline/wireless diversity OFDM systems using MRC. We have proved that the optimal subcarrier pairing is performed to sort the powerline subcarriers in ascending order of their SNRs and the wireless subcarriers in descending order of their SNRs. Further, the sorted subcarriers of both the powerline and wireless subcarriers are sequentially paired and the remaining powerline subcarriers with higher SNRs are used without pairing. We have observed from numerical results, that the proposed scheme achieves enhanced data rate and outage performance.

Chapter 5

Concluding Remarks

This dissertation has discussed the strategy to improve the reliability of the power line communications, which is considered as one of the most promising communication technology for Smart Grid. We especially has focused on broadband (BB) PLC operating on medium-voltage powerline networks.

5.1 Summary

We first considered an MRC diversity system for OFDM power line communication. From a simple mathematical inequality, an optimal subcarrier pairing scheme which maximizes the MRC gain was proposed. It was proved that the effective data subcarriers which are sorted in a descending order of their SNRs should be paired with the diversity sub-carriers which are sorted in an ascending order of their SNRs. Performance improvement of the proposed pairing scheme was verified in terms of symbol error rate (SER) by comparison with various other schemes for transmission via numerical results. MRC with optimal paring scheme always outperformed other schemes and the improvement in terms of SER due to diversity gain of optimal pairing was ranged from about tens of percent to several orders of magnitude according to the channel and noise

environments.

We also discussed a method to compensate the spectral loss which comes from the previous proposed subcarrier scheme due to the transmission of same data symbol twice. A precoding scheme proposed for wireless MIMO system which maximizes the minimum Euclidean distance $d_{\min}$ of the received constellation was applied to the PLC OFDM system. Numerical results showed that the adopted precoding scheme outperformed the MRC pairing scheme under the constraint of same transmission spectral efficiency. But the former required much higher computational complexity than the latter.

Next, we extended optimal subcarrier pairing with MRC approach to powerline/ wireless diversity system. Here, we assumed that a wireless network operates cooperatively with a powerline network. Similar to the results of subcarrier paring within PLC system in Chapter 3, the optimal subcarrier pairing in PLC/wireless diversity system is performed to sort the powerline subcarriers in ascending order of their SNRs and the wireless subcarriers in descending order of their SNRs. Numerical results showed that by optimally pairing subcarriers between two different communication systems, significant performance enhancement was achieved in terms of Ergodic data rate and outage probability.

5.2 Future Works

Throughout this dissertation, we focused on BB-PLC system for MV powerline networks. It is needed to verify the effectiveness of the proposed scheme in more various PLC candidates in Smart Grid such as NB-PLC in MV network, BB-PLC in MV network, and BB-PLC in LV network. As the powerline channel realization used for simulation was deterministic, time-varying channel characteristics also should be considered.

In Chapter 3, we briefly examined the SER performance variation with respect to

the ratio of the number of effective data subcarriers to the number of total subcarriers. The division of the subcarrier set into Γ^{eff} and Γ^{MRC} can be an optimization problem such as finding the optimal SNR threshold for division which maximizes the figure of merit, e.g., total data rate.

It was assumed that the subcarrier spacing of the powerline and wireless system was equivalent in Chapter 4. Proposed MRC pairing scheme can be extended to the case where the powerline and wireless systems comprise different OFDM parameters, which reflects more practical communication environments.

Moreover, we assumed that every subcarrier in PLC is modulated with the same constellation order. How to optimally combine the bit-loading algorithm with the proposed pairing scheme is a remaining problem.

Bibliography

[1] F. Bouhafs, M. Mackay, and M. Merabti, "Links to the future: communication requirements and challenges in the smart grid," *IEEE Power and Energy Magazine*, vol. 10, no. 1, pp. 24–32, January/February 2012.

[2] X. Yu, C. Cecati, T. Dillon, and M. G. Simões, "The new frontier of smart grids," *IEEE Industrial Electronics Magazine*, vol. 5, no. 3, pp. 49–63, September 2011.

[3] International Energy Agency (IEA), "Technology roadmap: smart grids," 2011. http://www.iea.org/topics/smartgrids/publications/ [URL]

[4] H. Farhangi, "The path of the smart grid," *IEEE Power and Energy Magazine*, vol. 8, no.1, pp. 18–28, January/February 2010.

[5] X. Fang, S. Misra, G. Xue, and D. Yang, "Smart grid — the new and improved power grid: a survey," *IEEE Communications Surveys & Tutorials*, vol. 14, no. 4, pp. 944–980, Fourth Quarter 2012.

[6] National Institute of Standards and Technology (NIST), "NIST framework and roadmap for smart grid interoperability standards, release 2.0," February 2012. http://www.nist.gov/smartgrid/upload/NIST_Framework_Release_2-0_corr.pdf [URL]

[7] V. C. Güngör, D. Sahin, T. Kocak, S. Ergüt, C. Buccella, C. Cecati, and G. P. Hancke, "Smart grid technologies: communication technologies and standards,"

IEEE Transactions on Industrial Informatics, vol. 7, no. 4, pp. 529–539, November 2011.

[8] V. C. Güngör, D. Sahin, T. Kocak, S. Ergüt, C. Buccella, C. Cecati, and G. P. Hancke, "A survey on smart grid potential applications and communication requirements," *IEEE Transactions on Industrial Informatics*, vol. 9, no. 1, pp. 28–42, Februray 2013.

[9] S. Galli, A. Scaglione, and Z. Wang, "For the grid and through the grid: the role of power line communications in the smart grid," *Proceeding of the IEEE*, vol. 99, no. 6, pp. 998–1027, June 2011.

[10] L. T. Berger, A. Schwager, J. J. Escudero-Garzas, "Power line communications for smart grid applications," *Journal of Electrical and Computer Enginneering*, vol. 2013, Article ID 712376, http://dx.doi.org/10.1155/2013/712376.

[11] W. Zhu, X. Zhu, E. Lim, and Y. Huang, "State-of-art power line communications channel modelling," *Procedia Computer Science*, vol. 17, pp. 563–570, 2013.

[12] M. Zimmermann and K. Dostert, "Analysis and modeling of impulsive noise in broad-band powerline communications," *IEEE Transactions on Electromagnetic Compatibility*, vol. 44, no. 1, 249–258, February 2002.

[13] M. Zimmermann and K. Dostert, "An analysis of the broadband noise scenario in powerline networks," in *Proceedings of the 4th International Symposium on Power Line Communications and its Applications (ISPLC 2000)*, Limerick, Ireland, 2000, pp. 131–137.

[14] V. Degardin, M. Lienard, A. Zeddam, F. Gauthier, and P. Degauque, "Classification and characterization of impulsive noise on indoor power lines used for data communications," *IEEE Transactions on Consumer Electronics*, vol. 48, no. 3, pp. 913–918, November 2002.

[15] T. Esmailian, F. R. Kschischang, and P. G. Gulak, "In-building power lines as high-speed communication channels: Channel characterization and a test channel ensemble," *International Journal of Communication Systems*, vol. 16, no. 5, pp. 381–400, May 2003.

[16] L. Lampe and A. J. Han Vinck, "Cooperative multihop power line communications," in *Proceedings of the 16th IEEE International Symposium on Power Line Communications and its Applications (ISPLC 2012)*, Beijing, China, March 2012, pp. 1–6.

[17] A. G. Lazaropoulos and P. G. Cottis, "Transmission characteristics of overhead medium-voltage power-line communications," *IEEE Transactions on Power Delivery*, vol. 24, no. 3, pp. 1164–1173, July 2009.

[18] H. Meng, S. Chen, Y. L. Guan, C. L. Law, P. L. So, E. Gunawan, and T. T. Lie, "Modeling of transfer characteristics for the broadband power line communication channel," *IEEE Transactions on Power Delivery*, vol. 19, no. 3, pp. 1057–1064, July 2004.

[19] P. Amirshahi and M. Kavehrad, "High-frequency characteristics of overhead multiconductor power lines for broadband communications," *IEEE Journal on Selected Areas in Communications*, vol. 24, no.7, pp. 1292–1303, July 2006.

[20] A. G. Lazaropoulos and P. G. Cottis, "Capacity of overhead medium voltage power line communication channels," *IEEE Transactions on Power Delivery*, vol. 25, no. 2, pp. 723–733, April 2010.

[21] Y.-H. Kim, S. Choi, S.-C. Kim, and J.-H. Lee, "Capacity of OFDM two-hop relaying systems for medium-voltage power-line access networks," *IEEE Transactions on Power Delivery*, vol. 27, no. 2, pp. 886–894, April 2012.

[22] OPERA1, "D5: pathloss as a function of frequency, distance and network topology for various LV and MV European powerline networks," IST Integrated Project No 507667, 2005.

[23] Z. Tao, Y. Xiaoxian, Z. Baohui, N. H. Xu, F. Xiaoqun, and L. Changxin, "Statistical analysis and modeling of noise on 10-kV medium-voltage power lines," *IEEE Transactions on Power Delivery*, vol. 22, no. 3, pp. 1433–1439, July 2007.

[24] H. C. Ferreira, L. Lampe, J. Newbury, and T. G. Swart, *Power Line Communications: Theory and Applications for Narrowband and Broadband Communications over Power Lines*, John Wiley & Sons, Chichester, West Sussex, United Kingdom, 2010.

[25] C. L. Giovaneli, B. Honary, and P. G. Farrell, "Space-frequency coded OFDM system for multi-wire power line communications," in *Proceedings of the 9th International Symposium on Power Line Communications and its Applications (ISPLC 2005)*, Vancouver, Canada, April 2005, pp. 191–195.

[26] J. Yoo and S. Choe, "MIMO-OFDM based broadband power line communication with maximum ratio combining," in *Proceedings of the 14th International Conference on Advanced Communications Technology (ICACT 2012)*, PyeongChang, South Korea, February 2012, pp. 774–777.

[27] _____. "MIMO-OFDM based indoor power line communication using spatial diversity coding and MRC schemes," in *Proceedings of the 18th Asia-Pacific Conference on Communications (APCC 2012)*, Jeju island, South Korea, October 2012, pp. 635–640.

[28] L. Cheng and H. C. Ferreira, "Time-diversity permutation coding scheme for narrow-band power-line channels," in *Proceedings of the 16th IEEE Interna-*

tional Symposium on Power Line Communications and its Applications (ISPLC 2012), Beijing, China, March 2012, pp. 120–125.

[29] K.-H. Kim, H. B. Lee, Y.-H. Kim, J.-H. Lee, and S.-C. Kim, "Cooperative multihop AF relay protocol for medium-voltage power-line-access network," *IEEE Transactions on Power Delivery*, vol. 27, no. 1, pp. 195–204, January 2012.

[30] D. Brennan, "Linear diversity combining techniques," *Proceedings of the IRE*, vol. 47, no. 6, pp. 1075–1102, June 1959.

[31] Y. Li, W. Wang, J. Kong, W. Hong, X. Zhang, and M. Peng, "Power allocation and subcarrier pairing in OFDM-based relaying networks," in *Proceedings of IEEE International Conference on Communications (ICC 2008)*, Beijing, China, May 2008, pp. 2602–2606.

[32] T. Wang, F. Glineur, J. Louveaux, and L. Vandendorpe, "Weighted sum rate maximization for downlink OFDMA with subcarrier-pair based opportunistic DF relaying," *IEEE Transactions on Signal Processing*, vol. 61, no. 10, pp. 2512–2524, May 2013.

[33] "First draft of the OPERA specification version 2", 2007 [Online]. Available: http://www.upaplc.org

[34] G. Caire, T. Y. Al-Naffouri, and A. Narayanan, "Impulsive noise cancellation in OFDM: an application of compressed sensings," in *Proceedings of IEEE International Symposium on Information Theory*, Toronto, Canada, July 2008, pp. 1293–1297.

[35] S.-J. Lee, D.-H. Shin, Y.-H. Kim, J.-J. Lee, and K.-H. Eom, "Analysis and modeling of noise on 22.9-kV underground power distribution cable for broadband power line communication," *International Journal of Control and Automation*, vol. 3, no. 3, pp. 1–12, September 2010.

[36] M. Kuhn and A. Wittneben, "PLC enhanced wireless access networks: a link level capacity consideration," *Proceedings the 55th IEEE Vehicular Technology Conference (VTC-Spring 2002)*, Bermingham, AL, USA, May 2002, pp. 125–129.

[37] L. Zheng and D. Tse, "Diversity and multiplexing: a fundamental tradeoff in multiple-antenna channels," *IEEE Transactions on Information Theory*, vol. 49, no. 5, pp. 1073–1096, May 2003.

[38] L. Collin, O. Berder, P. Rostaing, and G. Burel, "Optimal minimum distance-basde precoder for MIMO spatial multiplexing systems," *IEEE Transactions on Signal Processing*, vol. 52, no. 3, pp. 617–627, March 2004.

[39] E. Telatar, "Capacity of Multi-antenna Gaussian Channels," *European Transactions on Telecommunications*, vol. 10, no. 6, pp. 585–595, November-December 1999.

[40] B. Vrigneau, J. Letessier, P. Rostaing, L. Collin, and G. Burel, "Extension of the MIMO precoder based on the minimum euclidean distance: a corss-form matirx," *IEEE Journal of Selected Topics in Signal Processing*, vol. 2, no. 2, pp. 135–146, April 2008.

[41] Q. T. Ngo, O. Berder, B. Vrigneau, and O Sentieys, "Minimum distance based precoder for MIMO-OFDM systems using a 16-QAM modulation," in *Proceedings of IEEE International Conference on Communications (ICC 2009)*, Dresden, Germany, June 2009.

[42] D. Kapetanovic, H. V. Cheng, W. H. Mow, and F. Rusek, "Optimal two-dimensional lattices for precoding of linear channels," *IEEE Transactions on Wireless Communications*, vol. 12, no. 5, pp. 2104–2113, May 2013.

[43] M. Kuhn, S. Berger, I. Hammerström, and A. Wittneben, "Power line enhanced cooperative wireless communications," *IEEE Journal on Selected Areas in Communications*, vol. 24, no. 7, pp. 1401–1410, July 2006.

[44] S. W. Lai and G. G. Messier, "The wireless/power-line diversity channel," in *Proceedings of IEEE International Conference on Communications (ICC 2010)*, Cape Town, South Africa, May 2010.

[45] C. Jin and T. Kunz, "Smart home networking: lessons from combining wireless and powerline networking," *Smart Grid and Renewable Energy*, vol. 2, no. 2, pp. 136–151, May 2011.

[46] A. M. Sarafi, G. I. Tsiropoulos, and P. G. Cottis, "Hybrid wireless-broadband over power lines: a promising broadband solution in rural areas," *IEEE Communications Magazine*, vol. 47, no. 11, pp. 140–147, November 2009.

[47] J. G. Proakis, *Digital Communications,* 4th ed., McGraw-Hill, New York, NY, USA, 2001.

[48] V. Genc, S. Murphy, and J. Murphy, "Analysis of transparent mode IEEE 802.16j system performance with varying numbers of relays and associated transmit power," in *Proceedings of IEEE Wireless Communications and Networking Conference (WCNC 2009)*, Budapest, Hungary, April 2009.

[49] G. Senarath, M. Hart, S. Cai, et al., "Multi-hop relay system evaluation methodology (channel model and performance metric)," IEEE 802.16j-06/013, September 2006.

[50] M. Tlich, A. Zeddam, F. Moulin, and F. Gauthier, "Indoor power-line communications channel characterization up to 100 MHz—Part II: time-frequency analysis, " *IEEE Transactions on Power Delivery*, vol. 23, no.3, pp. 1402–1409, July 2008.

[51] V. Degardin, M. Lienard, A. Zeddam, F. Gauthier, and P. Degauque, "Classification and characterization of impulsive noise on indoor power lines used for data communications," *IEEE Transactions on Consumer Electronics*, vol. 48, no. 4, pp. 913-918, November 2002.

[52] T. V. Prasad, S. Srikanth, C. N. Krishnan, and P. V. Ramakrishna, "Wideband characterization of low voltage outdoor powerline communication channels in India," in *Proceedings of the 5th International Symposium on Power Line Communications and its Applications (ISPLC 2001)*, Malmö, Sweden, April 2001, pp. 359–364.

Chapter A

Coherence Bandwidth of Powerline Channel

Characterization of wideband channel performance subject to multipath can be usefully described using the coherence bandwidth [50]. The frequency-selective behavior of the channel can be described in terms of the autocorrelation function for a wide sense stationary uncorrelated scattering (WSSUS) channel. Equation (A.1) gives $R(\Delta f)$, the Frequency Correlation Function (FCF):

$$R(\Delta f) = \int_{-\infty}^{\infty} H(f)H^*(f+\Delta f)df \tag{A.1}$$

where $H(f)$ is the channel transfer function (CTF), Δf is the frequency shift and $*$ denotes the complex conjugate. $R(\Delta f)$ is a measure of the magnitude of correlation between the channel response at two spaced frequencies. The coherence bandwidth is a statistical measure of the range of frequencies over which the FCF can be considered "flat" (i.e., a channel passes all spectral components with approximately equal gain and linear phase). In other words, coherence bandwidth is the range of frequencies over which two frequency components have a strong potential for amplitude correlation.

No single definitive value of correlation has emerged for the specification of coherence bandwidth. Hence, coherence bandwidths for generally accepted values of correlations coefficient equal to 0.5, 0.7, and 0.9 were evaluated from each FCF, and

these are referred to as $B_{0.5}$, $B_{0.7}$, and $B_{0.9}$, respectively.

In [51], the coherence bandwidth at 0.9 correlation level for the 1–30 MHz frequency band, was observed to have an average value of 1 MHz. The minimum estimated value of $B_{0.9}$ for the 0.5–15 MHz frequency band was 25 kHz in [52]. In [50], various statistics of the coherence bandwidth were obtained according to the correlation levels: for example, the minimum value of $B_{0.9}$, the maximum value of value of $B_{0.9}$, and the mean value of $B_{0.9}$ was about 44 kHz, 1.9 MHz, and 310 kHz, respectively, for the 2–100 MHz frequency band.

Chapter B

Independence Between Pair of Subcarriers within PLC System

As far as the subcarrier pairing within the same communication system such as in Chapter 3 is concerned, the independence between two subcarriers which comprise each subcarrier pair should be maintained to make the proposed pairing scheme meaningful. This independence is related to the coherence bandwidth of the channel.

In advance, the subcarrier spacing which is smaller than the coherence bandwidth makes the individual subcarrier in OFDM system experiences flat-fading over a frequency-selective fading channel. About 20 kHz of subcarrier spacing in the considered system satisfies the whole range of the coherence bandwidth of the powerline channel mentioned in Appendix A.

In contrast, the frequency separation between subcarriers to be paired with each other should be larger than the coherence bandwidth for independence. That is, for subcarrier pair (i, j) where $i \in \Gamma_{\text{eff}}$ and $j \in \Gamma_{\text{MRC}}$,

$$|f^{(i)} - f^{(j)}| = |i - j| \cdot \Delta f > B_c. \tag{B.1}$$

The ratio of the number of subcarrier pairs where the frequency separation between

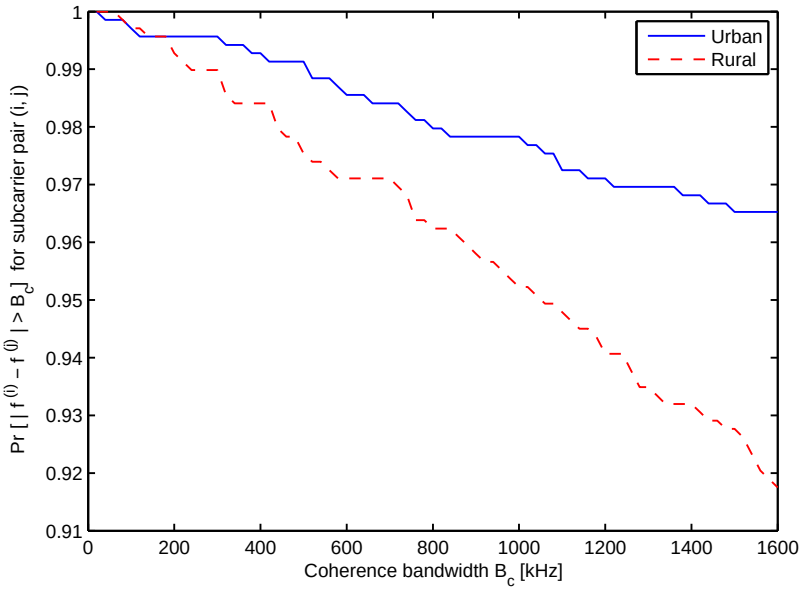

Figure B.1: Probability satisfying the independence condition (B.1) with respect to the value of the coherence bandwidth.

subcarriers is larger than the coherence bandwidth to the total number of subcarrier pairs is depicted in Figure B.1. As shown in the figure, almost all subcarrier pairs satisfy the independence condition (B.1) especially with a smaller value of the coherence bandwidth, but more than 91 % of the subcarrier pairs still satisfies the condition in the worst case.

국문초록

지구 온난화, 증가하는 에너지 요구 및 최대 부하에 따른 위험 문제 등을 해결하기 위해, 스마트 그리드 구축을 위한 많은 노력들이 진행 중이다. 스마트 그리드를 구현하기 위해서는 향상된 정보통신 기술이 필요하며, 이는 통신 네트워크를 통한 안정성 있는 데이터 전송 여부에 달려있다. 스마트 그리드를 위한 여러 통신기술 후보 중 전력선통신 (PLC), 특히 중전압 (MV) 전력선 상의 고속 PLC에 집중하였다. 전력선 통신 네트워크의 신뢰성은 전력선이 스마트 그리드의 통신 매체로 올바르게 동작하기 위한 선결 조건이다.

본 논문에서는 전력선 통신을 보다 신뢰성 있고 강건하게 만들기 위한 방안에 대하여 연구한다. 이를 위해 OFDM 기반의 전력선 통신 시스템에서 최대비합성 (MRC) 다이버시티 구조를 고안한다. 이러한 시스템에서 최대비합성 다이버시티 이득을 최대화하기 위한 최적의 부반송파 페어링 (subcarrier pairing) 기법을 제안한다. 모의실험을 통해 제안하는 기법의 성능 향상 여부를 검증한다.

다이버시티 이득은 주파수 효율의 감소를 유발한다. 앞의 제안된 부반송파 페어링 기법으로 인해 본질적으로 발생하는 주파수 효율 감소를 해결하기 위해, 무선 MIMO 채널의 전처리 (precoding) 기법을 적용한다. 모의실험 결과를 통해, 높은 변조 지수로 페어링 기법을 이용하는 것이 매우 많은 계산량이 필요한 전처리 기법과 비교하여 유사한 성능을 나타냄을 알 수 있다.

다음으로 최대비합성 기반 최적 부반송파 페어링 기법을 전력선/무선 다이버시티 시스템에 확장한다. 이 시스템에서 전력선과 무선시스템의 각 부반송파들은 짝을 이루어 최대비합성을 수행한다. 전체 데이터 전송률을 최대화하기 위해 앞과 유사한 최적 부반송파

페어링 기법을 제안한다. 모의실험 결과를 통해 제안된 기법이 데이터 전송률과 아웃티지 확률 측면에서 상당한 성능 향상을 나타낸다.

주요어 : 스마트 그리드, 전력선 통신, 신뢰성, 다이버시티, 최대비합성, 부반송파 페어링
학 번 : 2004–21537